Article

Cell

A Creatine-Driven Substrate Cycle Enhances Energy Expenditure and Thermogenesis in Beige Fat

Graphical Abstract

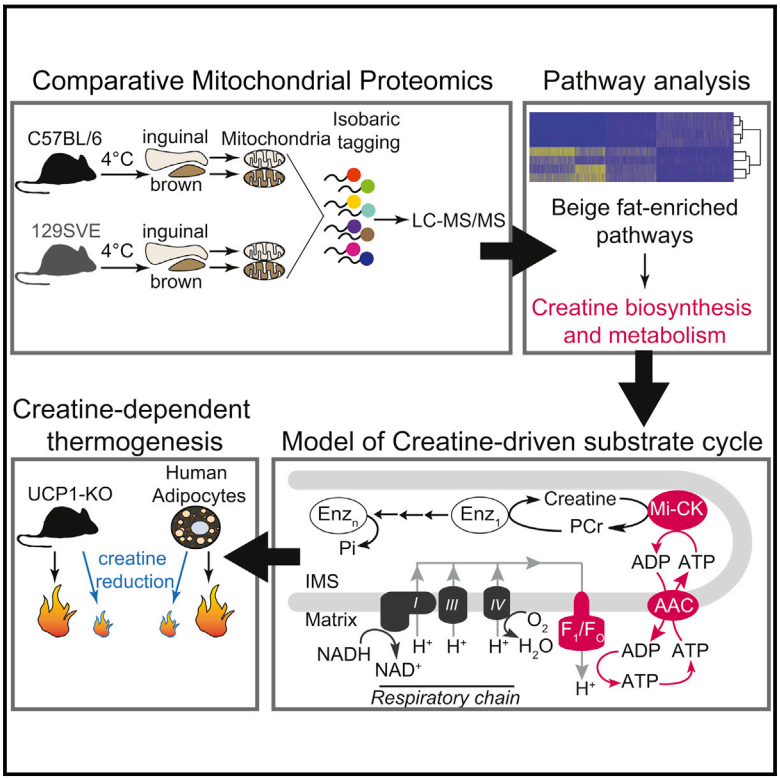

Highlights

- Quantitative proteomics identifies a creatine enzyme signature in beige fat
- Creatine-driven substrate cycling enhances beige-fat mitochondrial respiration
- Genes and proteins of creatine metabolism exhibit a reciprocal relationship with Ucp1
- Creatine reduction decreases energy expenditure in mice and human brown adipocytes

Authors

Lawrence Kazak, Edward T. Chouchani, Mark P. Jedrychowski, ..., Shingo Kajimura, Steve P. Gygi, Bruce M. Spiegelman

Correspondence

bruce_spiegelman@dfci.harvard.edu

In Brief

Beige fat uses creatine to dissipate energy and stimulate mitochondrial ATP demand, thereby promoting cold adaptation.

Kazak et al., 2015, Cell *163*, 643–655
October 22, 2015
http://dx.doi.org/10.1016/j.cell.2015.09.035

CellPress

Article

Cell

A Creatine-Driven Substrate Cycle Enhances Energy Expenditure and Thermogenesis in Beige Fat

Lawrence Kazak,[1,2] Edward T. Chouchani,[1,2] Mark P. Jedrychowski,[2] Brian K. Erickson,[2] Kosaku Shinoda,[3] Paul Cohen,[1,2] Ramalingam Vetrivelan,[4] Gina Z. Lu,[1] Dina Laznik-Bogoslavski,[1] Sebastian C. Hasenfuss,[1,2] Shingo Kajimura,[3] Steve P. Gygi,[2] and Bruce M. Spiegelman[1,2,*]

[1]Dana-Farber Cancer Institute, Boston, MA 02115, USA

[2]Department of Cell Biology, Harvard University Medical School, Boston, MA 02115, USA

[3]Diabetes Center, University of California, San Francisco (UCSF), San Francisco, CA 94143, USA

[4]Department of Neurology, Harvard Medical School and Beth Israel Deaconess Medical Center, Boston, MA 02215, USA

*Correspondence: bruce_spiegelman@dfci.harvard.edu

http://dx.doi.org/10.1016/j.cell.2015.09.035

SUMMARY

Thermogenic brown and beige adipose tissues dissipate chemical energy as heat, and their thermogenic activities can combat obesity and diabetes. Herein the functional adaptations to cold of brown and beige adipose depots are examined using quantitative mitochondrial proteomics. We identify arginine/creatine metabolism as a beige adipose signature and demonstrate that creatine enhances respiration in beige-fat mitochondria when ADP is limiting. In murine beige fat, cold exposure stimulates mitochondrial creatine kinase activity and induces coordinated expression of genes associated with creatine metabolism. Pharmacological reduction of creatine levels decreases whole-body energy expenditure after administration of a β3-agonist and reduces beige and brown adipose metabolic rate. Genes of creatine metabolism are compensatorily induced when UCP1-dependent thermogenesis is ablated, and creatine reduction in *Ucp1*-deficient mice reduces core body temperature. These findings link a futile cycle of creatine metabolism to adipose tissue energy expenditure and thermal homeostasis.

INTRODUCTION

Non-shivering thermogenesis primarily takes place in brown and beige adipose tissues. The ability of these depots to dissipate chemical energy has led to interest in their ability to combat obesity and diabetes. The thermogenic property of brown and beige fat relies predominantly on the actions of uncoupling protein 1 (UCP1) (Cannon and Nedergaard, 2004). This protein resides in the mitochondrial inner membrane and stimulates thermogenesis by dissipating the protonmotive force (Δp) and increasing the rate of substrate flux through the mitochondrial respiratory chain.

It is now appreciated that there are at least two distinct UCP1-expressing cell types. Classical brown adipocytes are derived from a *Myf5*$^+$ lineage and are located primarily in developmentally formed depots in the interscapular region of rodents and human infants (Seale et al., 2008). Beige-fat cells arise primarily from a *Myf5*$^-$ lineage and generally accumulate in white fat depots upon cold challenge or with the application of a number of different adrenergic stimuli, hormones, and peptide factors. Much (but probably not all) of the "brown fat" of adult humans in the neck and supraclavicular areas has the molecular characteristics of beige fat, rather than those of the classical brown fat of rodents (Shinoda et al., 2015; Wu et al., 2012). On the other hand, the interscapular depots of human infants do indeed resemble the classical brown fat of rodents (Lidell et al., 2013).

Ablation experiments in mice have shown that UCP1$^+$ cells, taken as a whole, protect mice from the metabolic effects of high-fat feeding. Diminution of UCP1$^+$ cells via transgenic expression of a toxigene first established the key role of these cells in the regulation of metabolic health (Lowell et al., 1993). Mice with *Ucp1* deletion also develop obesity, although in this case obesity is only observed at thermoneutrality (Feldmann et al., 2009). Recently, beige-fat function has been ablated in mice, with classical brown-fat function left largely intact (Cohen et al., 2014); these animals develop moderate obesity and insulin resistance centered on the liver.

The realization that mammals have two distinct thermogenic cell types raises questions regarding their similarities and their differences. Questions concerning fuel preferences, hormone sensitivities, and other key thermogenic pathways and functions are largely unexplored. We have performed quantitative proteomics, comparing highly purified mitochondria from brown and beige-fat depots. The results indicate that beige-fat cells have a thermogenic mechanism built around a creatine-driven substrate cycle.

RESULTS

Mitochondrial Purification from Cold-Exposed Brown and Beige Fat

We set out to compare the proteomic and bioenergetic properties of mitochondria isolated from beige and brown adipose tissue upon induction of thermogenesis through cold exposure. To this end, we exposed mice to 4°C, which is sufficient to drive thermogenesis in subcutaneous inguinal white adipose tissue (iWAT) and classical interscapular brown adipose tissue (BAT).

We used western blotting to evaluate the purity of our mitochondrial preparations. As expected, mitochondrial proteins were enriched, whereas contaminating components of the cytoplasm and endoplasmic reticulum were largely removed during the purification procedure (Figures S1A and S1B). Mitochondrial yield increased substantially (beige: 10-fold and brown: 2-fold) following cold exposure (Figure S1C). These mitochondria from both sources displayed properties indicative of UCP1^{+} organelles, including the requirement for BSA and purine nucleotides to acquire respiratory control (Figure S1D). These data are in line with previous reports (Shabalina et al., 2013) and indicate that beige-fat mitochondria from iWAT are functionally thermogenic following cold exposure.

Quantitative Mitochondrial Proteomics Identifies Arginine/Creatine Metabolism as a Signature of Beige Adipose Tissue

We used tandem mass spectrometry after isobaric peptide tagging to identify protein species exhibiting differential abundance between beige and brown adipose mitochondria from two strains (C57BL/6 and 129SVE) of cold-exposed mice (Figure 1A and Table S1). As shown by the global heatmap (Figure 1B) and the principal-component analysis (Figure 1C), brown-fat mitochondria showed marginal strain-dependent variance, whereas beige-fat mitochondria demonstrated greater diversity across strains. Next, beige and brown-fat mitochondrial proteomes were stratified according to differential relative abundance (Figure 1B), followed by identification of beige-fat-selective biological pathways (Figure 1D). Because mitochondrial proteins made up a larger percentage of the material after isolating pure organelles through a sucrose gradient, relative to crude mitochondria obtained by differential centrifugation alone (Figures S1A and S1B), we defined bona fide mitochondrial proteins to be those with higher abundance in the pure fraction, relative to the crude fraction. Thus, protein abundance between crude and pure preparations of mitochondria from beige and brown fat was examined by mass spectrometry (Figure 1E and Table S2). Proteins that had higher abundance in pure mitochondria, relative to crude mitochondria, were cross-referenced to the initial proteomics inventory (Table S1). Pathway analysis demonstrated that components of arginine-dependent creatine and proline metabolism were reproducibly enriched in beige-fat relative to brown-fat mitochondria (Figures 1D and 1F). A total of 14 proteins were identified that could be assigned to this pathway (Table S3). Enzymes with the ability to synthesize creatine and remove ornithine, an inhibitor creatine biosynthesis (Sipilä, 1980), showed beige-fat selectivity (Figure 1G). There was a strong correlation between western blotting and proteomic quantification for beige- and brown-enriched mitochondrial proteins (Figures S1E–S1G). Increased protein abundance in beige-fat mitochondria was observed for components of arginine-dependent creatine and proline metabolism, such as GATM and CKMT2, as well as the majority of ATP synthase subunits (Figure 1H and Table S1). Beige-fat mitochondria contained higher levels of creatine kinase (CK) activity relative to brown-fat mitochondria in both C57BL/6 and 129SVE strains of mice following cold exposure (Figure S1H). Moreover, mitochondrial CK activity was cold inducible (~2-fold) in beige fat (Figure 1I).

Given that creatine metabolism was found to be a distinct feature of thermogenic beige adipocytes at the protein level, we monitored changes in the mRNA expression of genes involved in creatine metabolism following 6 hr and 1 week exposure to 4°C. Transcript levels of these genes were coordinately elevated in response to cold in iWAT but not in BAT (Figure 1J). *Gatm* and *Ckmt1* transcript abundance was similar between iWAT and BAT. However, GATM and CKMT1 protein expression was higher in beige-fat than in brown-fat mitochondria (Table S3). In contrast, *Ckmt2* transcript levels were greater in BAT compared to iWAT. However, the expression level of CKMT2 protein was found to be slightly greater in beige-fat than in brown-fat mitochondria (Figure 1H and Table S3). The discordance between *Ckmt2* mRNA from whole-tissue lysates and protein abundance from isolated mitochondria is likely due to higher mitochondrial content in BAT than iWAT.

We next investigated the levels of creatine and phosphocreatine (PCr) in iWAT and BAT from mice housed at 30°C or 4°C. Creatine levels in iWAT were elevated 2-fold following cold exposure (Figure S1I). In contrast, although higher steady-state creatine levels were observed in BAT, cold exposure had no detectable effect (Figure S1I). There was no difference in PCr levels in either iWAT or BAT in response to cold (Figure S1J), although a modest trend toward lower PCr levels in BAT was observed; these observations are in line with a recent report (Grimpo et al., 2014). As a consequence of these measurements, it is clear that the PCr/creatine ratio in iWAT was reduced significantly in cold-exposed animals (Figure 1K), suggesting increased creatine metabolism in beige fat. These changes in creatine levels were not observed in skeletal muscle of the same animals (Figure S1K).

Creatine Stimulates Respiration in Beige-Fat Mitochondria when ADP Is Limiting

Based on our identification of creatine metabolism as a signature of beige-fat mitochondria and due to the functional coupling of mitochondrial CK (Mi-CK) to oxidative phosphorylation through the ATP/ADP carrier (AAC) (Jacobus and Lehninger, 1973; Wyss and Kaddurah-Daouk, 2000), we posited that creatine could dissipate the mitochondrial ATP pool to drive ADP-dependent respiration in beige-fat mitochondria. Such a pathway would require creatine and CK-mediated hydrolysis of ATP to drive a catalytic mechanism that stimulates cycling of ATP production and consumption (Figure 2A). We therefore tested whether creatine could stimulate substrate cycling and increase ADP-dependent respiration in beige-fat mitochondria.

Striated muscle tissues are understood to utilize creatine metabolism such that mitochondrial ATP and creatine generate PCr and ADP in a 1:1 stoichiometry (Wyss and Kaddurah-Daouk, 2000). The resulting PCr pool is used to drive substrate-level phosphorylation of ADP during times of ATP deficit. Thus, a direct prediction of this classical metabolic utilization of PCr is that addition of a quantity of creatine to oxidatively coupled mitochondria will result in a molar equivalent production of ADP and PCr through CK-mediated phosphotransferase activity (Jacobus and Lehninger, 1973). Alternatively, if creatine drives futile substrate cycling, addition of a given

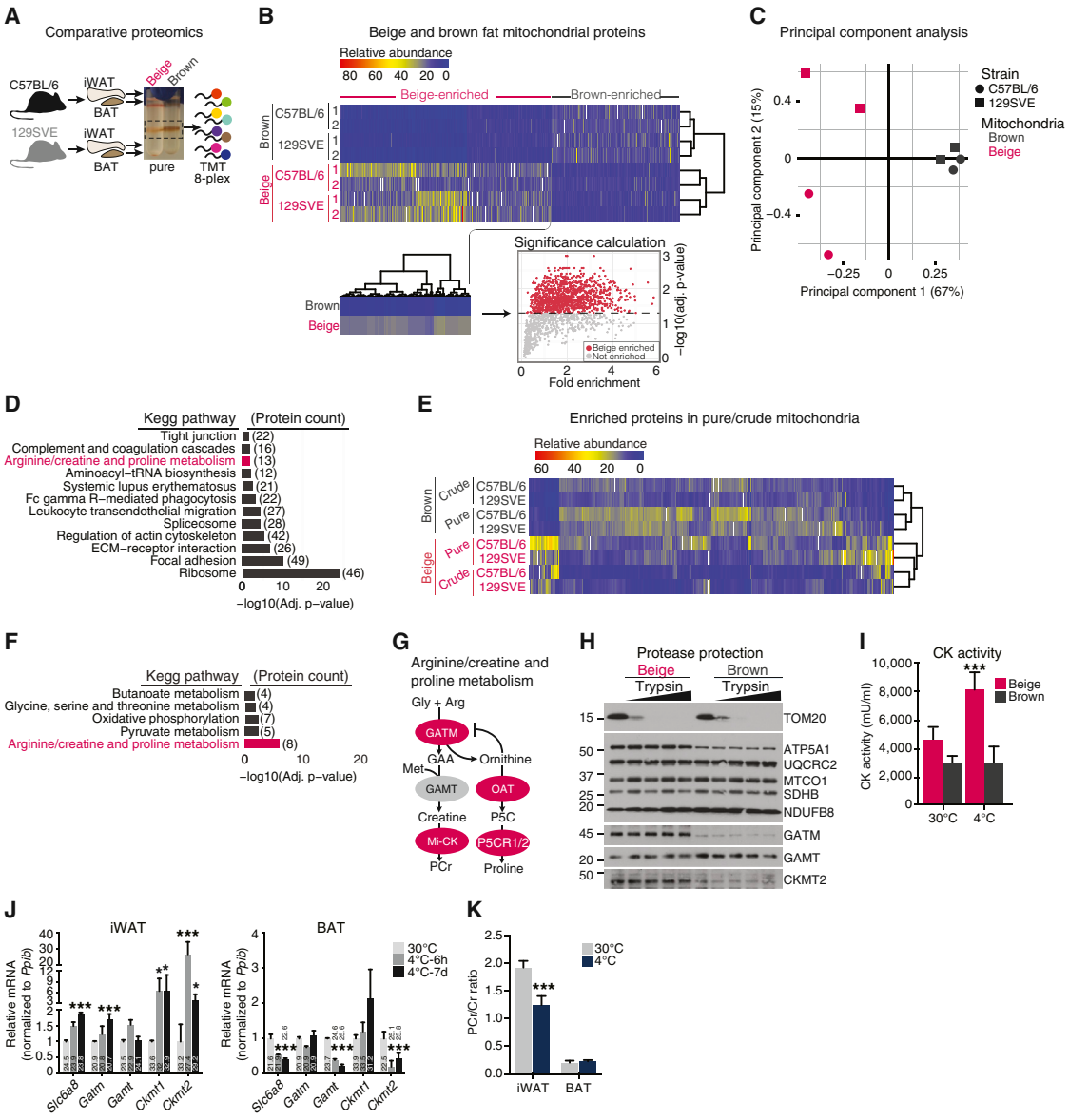

Figure 1. Characterization of Mitochondria from Brown and Beige Adipose Tissues

(A) Schematic of mitochondrial purification and quantitative proteomics workflow.

(B) Heatmap of beige-fat and brown-fat mitochondrial proteomics data (from Table S1). Beige-enriched proteins are shown in the subset heatmap.

(C) Principal-component analysis of the mitochondrial proteomics dataset.

(D) Kegg pathway analysis of beige-fat-selective mitochondrial proteins from Figure 1B.

(E) Heatmap of beige-fat and brown-fat mitochondrial proteomics data (from Table S2) after selecting proteins on the basis of an expression ratio greater than 1 in pure/crude mitochondria.

(F) Kegg pathway analysis of significantly enriched beige-fat mitochondrial proteins after cross-referencing Tables S1 and S2.

(G) Schematic of creatine synthesis and byproduct removal proteins identified by mass spectrometry. Red circles, proteins identified by mass spectrometry; gray circles, proteins not identified. Gly, glycine; Arg, arginine; Met, methionine; PCr, phosphocreatine; P5C, 1-pyrroline-5-carboxylic acid; Mi-CK, mitochondrial CK.

(H) Western blot after treatment of beige- and brown-fat mitochondria with trypsin (0, 10, 25, 50, and 100 μg ml^{-1}).

(I) CK activity of mitochondria from 129SVE mice housed at 30°C or 4°C for 7 days.

(J) Quantitative RT-PCR (qRT-PCR) from C57BL/6 mice housed at 30°C or 4°C for 6 hr (4°C—6 hr) or 7 days (4°C—7 days); n = 3 to 4 mice per group.

(K) PCr to creatine (Cr) ratio in iWAT and BAT from 129SVE mice housed at 30°C or 4°C for 7 days.

Data are presented as means ± SEM. *p < 0.05, ***p < 0.01.

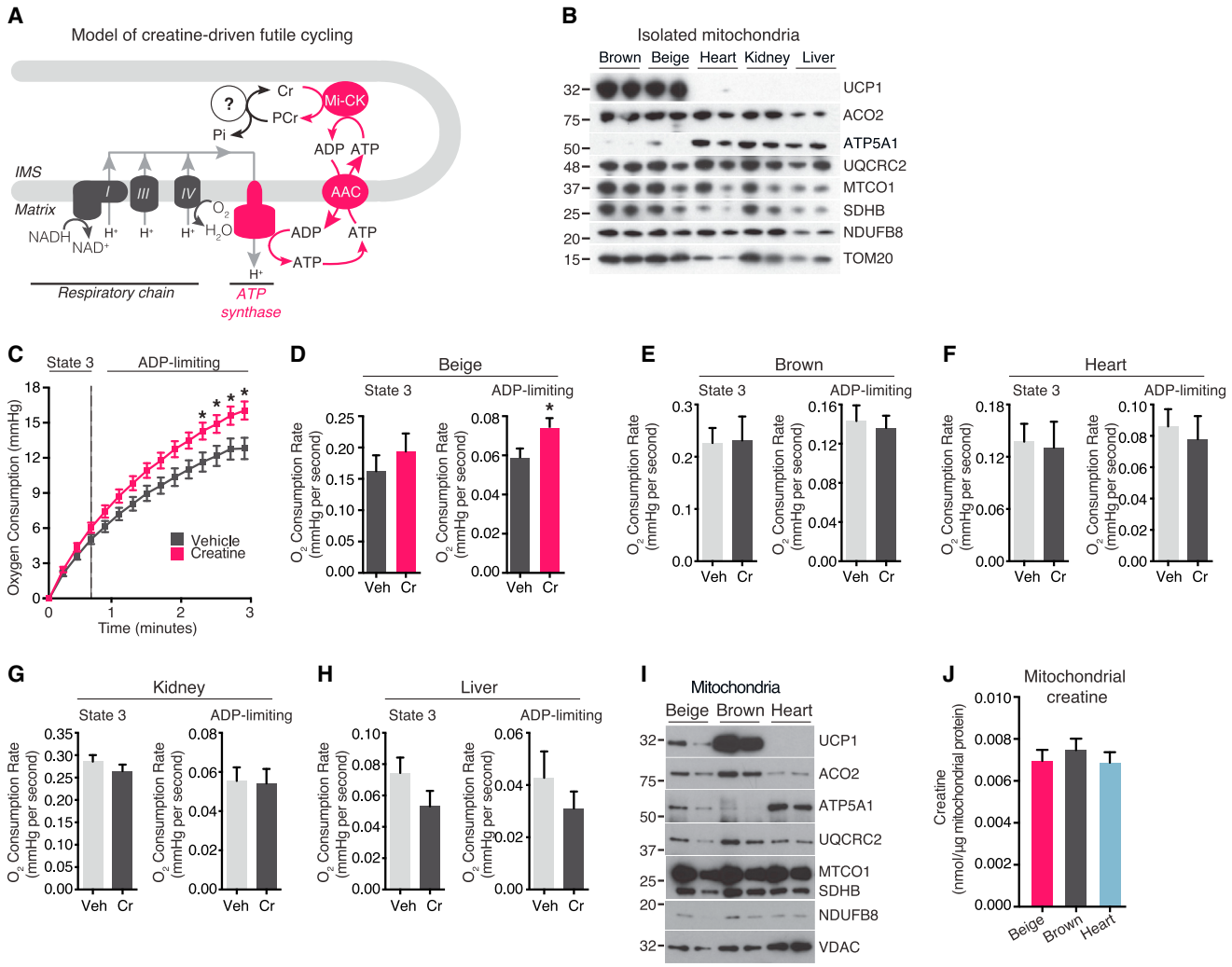

Figure 2. Creatine Stimulates Respiration in Beige-Fat Mitochondria when ADP Is Limiting

(A) Model of creatine-based substrate cycling. IMS, intermembrane space; AAC, ADP/ATP carrier.

(B) Western blot of mitochondrial proteins. n = 2 mitochondrial preparations, 15 mice per cohort.

(C) Oxygen consumption by beige-fat mitochondria treated with and without creatine (0.01 mM) in the presence of 0.2 mM ADP. Vertical dashed line, state 3 to state 4 transition. n = 9 mitochondrial preparations, 15 mice per cohort.

(D) State 3 and ADP-limiting oxygen consumption rate (OCR) of beige-fat mitochondria treated with and without creatine in the presence of 0.2 mM ADP. n = 9 mitochondrial preparations, 15 mice per cohort.

(E) State 3 and ADP-limiting OCR of brown-fat mitochondria treated as in (D). n = 3 mitochondrial preparations, 15 mice per cohort.

(F) State 3 and ADP-limiting OCR of heart mitochondria treated as in (D). n = 3 mitochondrial preparations, 8 mice per cohort.

(G) State 3 and ADP-limiting OCR of kidney mitochondria treated as in (D). n = 3 mitochondrial preparations, 15 mice per cohort.

(H) State 3 and ADP-limiting OCR of liver mitochondria treated as in (D). n = 3 mitochondrial preparations, 2 mice per cohort.

(I) Western blot of mitochondrial proteins from beige fat, brown fat, and heart. n = 2 mitochondrial preparations, 15 mice per cohort.

(J) Mitochondrial creatine concentration in beige fat, brown fat, and heart.

Data are presented as means ± SEM. *p < 0.05.

amount of creatine would instead drive the release of a molar excess of ADP with respect to creatine, thus resulting in a surplus of oxygen consumption if ADP is limiting. In this case, the relationship of creatine to ADP liberation would be substoichiometric.

The stoichiometric relationship between creatine and ATP synthase-coupled respiration was examined in mitochondria isolated from a panel of tissues. Western blotting demonstrated similar mitochondrial yields from brown fat, beige fat, heart, kidney, and liver (Figure 2B). Mitochondria were respired on pyruvate and malate in the presence of varying ADP concentrations. These organelles exhibited the expected behavior on addition of sub-saturating amounts of ADP (0.01–0.2 mM), such that respiration transitioned to state 4 as ADP became limiting (Figures S2A and S2B). In contrast, a saturating amount of ADP (1 mM) resulted in state 3 respiration with no transition to state 4, as

ADP was no longer limiting over the course of the incubation (Figure S2A).

In the presence of sub-saturating levels of ADP, addition of a sub-stoichiometric amount of creatine (0.01 mM) stimulated an ~30% increase in respiration in beige-fat mitochondria. Specifically, creatine did not significantly affect the initial (state 3) ADP-stimulated rate of oxygen consumption (Figures 2C and 2D, left panel) but enhanced the respiration rate when ADP levels became limiting (Figures 2C and 2D, right panel). This action of creatine in beige-fat mitochondria did not occur in the absence of exogenous ADP (Figure S2C) nor did it occur in the presence of the AAC inhibitor, carboxyatractyloside (Figure S2D). These data suggest that creatine-mediated respiration required export of mitochondrial matrix ATP through the AAC upon addition of exogenous ADP (Figure 2A). This feature of creatine-dependent respiration is in agreement with the established functional coupling of AAC with Mi-CK isoforms (Jacobus and Lehninger, 1973; Wyss and Kaddurah-Daouk, 2000). Furthermore, incubation of beige-fat mitochondria with saturating ADP concentrations (Figure S2E) precluded the respiration-stimulating effects of creatine (Figure S2F), further confirming that the stimulatory effects occurred only under ADP-limiting conditions.

On the basis of the mitochondrial P/O ratio (Watt et al., 2010) we calculated the amount of additional ATP that was synthesized by addition of creatine to beige-fat mitochondria. Creatine drove an increase in oxygen consumption equivalent to a 7.82-fold (±2.12) excess phosphorylation of ADP. These results indicate that in beige adipose mitochondria, creatine acts substoichiometrically (with respect to ADP phosphorylation) to increase mitochondrial ATP synthesis and stimulate substrate flux through the mitochondrial respiratory chain. Addition of sub-stoichiometric amounts of creatine to mitochondria isolated from brown fat, heart, kidney, or liver (Figure 2B) had no effect on ADP-dependent respiration (Figures S2G and 2E–2H).

Striated muscle contains a large quantity of creatine (Fitch and Chevli, 1980), and so endogenous mitochondrial creatine levels in beige and brown fat were compared to heart following purification of a comparable yield of organelles from these tissues (Figure 2I). Figure 2J demonstrates that mitochondrial creatine levels were similar between tissues following purification, indicating that the lack of a respiration-enhancing effect in heart mitochondria was not due to a high amount of endogenous creatine. Together, these data indicate that creatine stimulates respiration in beige-fat mitochondria in a substoichiometric manner with respect to ADP, specifically when ADP is limiting; this is consistent with a model of creatine-driven substrate cycling (Figure 2A).

To examine thermogenesis by creatine-driven substrate cycling, we employed differential scanning calorimetry (Ricquier et al., 1979). As expected, chemical uncoupling by FCCP induced thermogenesis, and this signal was inhibited by rotenone and antimycin; the signal was similar to that obtained when mitochondria were omitted from the reaction (Figure S2H). Importantly, addition of creatine to beige-fat mitochondria drove ADP-dependent thermogenesis by ~30% relative to organelles incubated with ADP alone (Figure S2I). This is a direct demonstration of thermogenesis through creatine metabolism in beige-fat mitochondria.

Creatine Metabolism in Adipose Tissue Contributes to Energy Expenditure and Thermal Homeostasis In Vivo

As the role of creatine metabolism in thermogenic fat tissues is essentially unexplored in vivo, we systematically assessed its role in beige and brown adipose metabolic functions. First, we examined whether creatine regulates oxidative metabolism in beige and brown fat. To this end, we utilized β-guanidinopropionic acid (β-GPA), a creatine analog that is well established to inhibit creatine transport and to reduce creatine levels in cultured cells and tissues (Fitch and Chevli, 1980). A diet supplemented with a typical dose of β-GPA (2%), resulted in reductions in food intake and weight loss, as previously reported (Oudman et al., 2013); this compromised subsequent metabolic analyses. However, when mice were given daily intraperitoneal injections with a lowered dose of β-GPA (0.4 g kg^{-1}) for 4 days during cold exposure, body weight and fat-pad weight were unaffected (Figures S3A and S3B). Creatine levels were reduced by approximately 50% in iWAT and BAT and by 15% in gastrocnemius muscle (Figure 3A). Mitochondrial respiratory chain protein expression was not altered (Figure 3B). To determine the contribution of creatine metabolism in brown/beige adipose to whole-body energy expenditure, we utilized the β3-adrenergic receptor agonist CL 316,243 (CL), a well-known activator of adipose thermogenesis (Bloom et al., 1992; Granneman et al., 2003). Movement, food intake, and oxygen consumption were monitored in CL-treated mice that were co-treated with either vehicle or β-GPA. There was no difference in ambulatory movement, food intake, or fuel utilization between vehicle- or β-GPA-treated animals (Figures 3C, 3D, and S3C). As expected, we detected a 54% increase in the metabolic rate of mice following CL injection. Strikingly, a reduction in creatine through the administration of β-GPA diminished the CL-induced increase in whole-body oxygen consumption by ~40% compared to vehicle treatment (Figure 3E).

The reduction in whole-body oxygen consumption prompted an examination of which tissues were most affected by β-GPA, in terms of whole-tissue respiration. Thus, another cohort of mice, housed at 23°C, was separated into four groups: vehicle, β-GPA, CL, or CL + β-GPA. β-GPA had no effect on the respiration of any tissue examined in the absence of a browning stimulus (Figure 3F). CL treatment provided a powerful browning/beiging stimulus, resulting in a 5-fold increase in iWAT oxygen consumption, a 33% increase in BAT respiration, a 9-fold elevation in PgWAT respiration, and no effect on Gstrc respiration (Figure 3F). Reducing creatine levels with β-GPA had a profound and significant effect on beige iWAT, resulting in a 34% reduction in oxygen consumption (Figure 3F). BAT oxygen consumption was reduced by 18% following β-GPA treatment, PgWAT oxygen consumption was decreased by 15%, and no detectable effect on Gstrc tissue respiration was detected (Figure 3F). Although the β-GPA-dependent reduction in BAT respiration did not reach statistical significance, the absolute decrease was larger than any other tissue examined, and so in addition to iWAT, BAT may well contribute to the effects of β-GPA observed in vivo.

We next examined the contribution of beige adipocytes within iWAT to creatine-dependent oxidative metabolism. Mice with an adipose-selective deletion of *Prdm16* (Adipo-PRDM16 KO) have disrupted beige adipose function (Cohen et al., 2014). Following

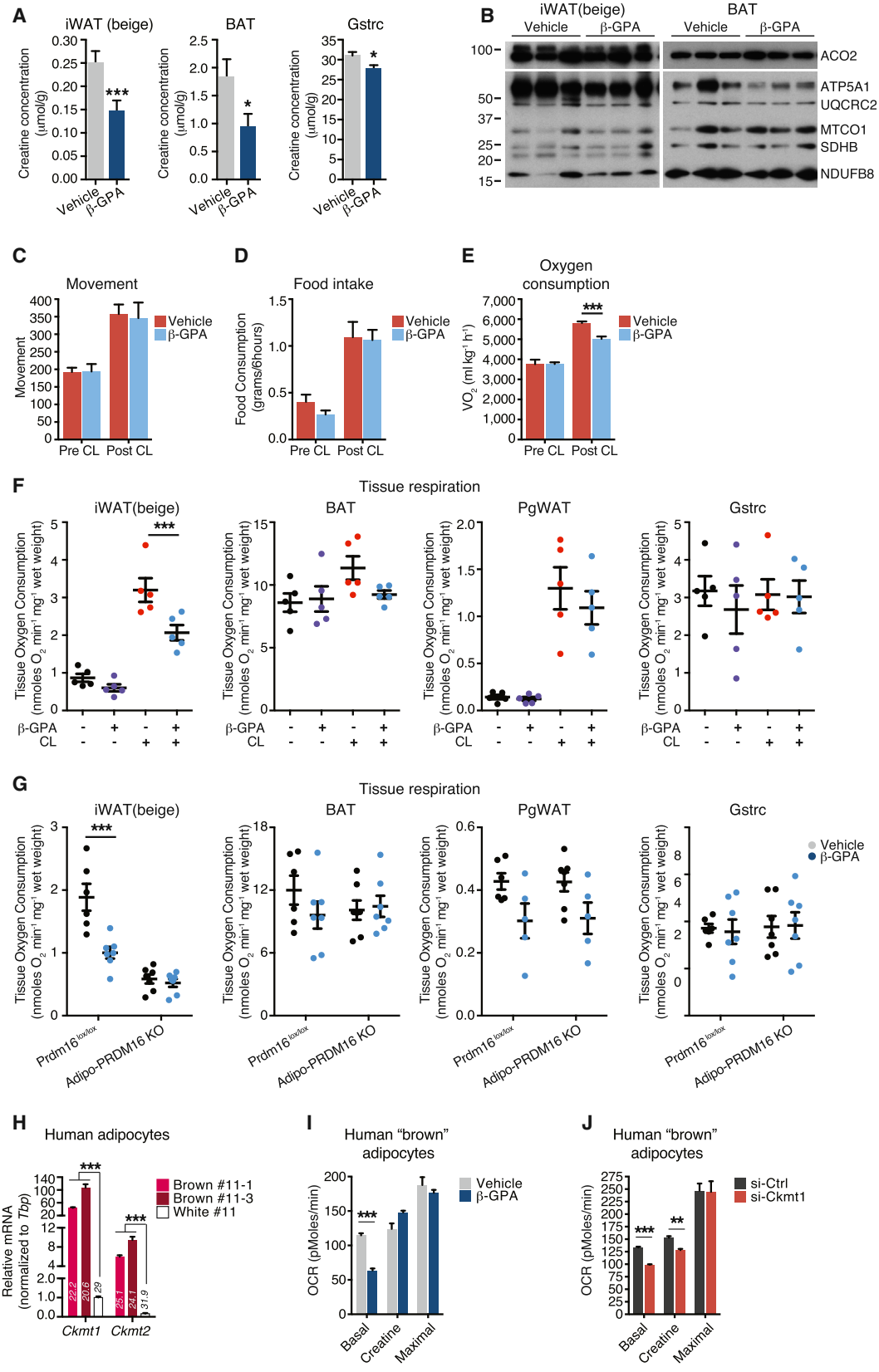

(legend on next page)

7 days of cold exposure, creatine reduction with β-GPA significantly decreased iWAT oxidative metabolism from control *Prdm16*$^{lox/lox}$ mice but had no further effect on the already reduced respiratory rate of iWAT from Adipo-PRDM16 KO mice (Figure 3G). No significant effect of creatine reduction was detected in any other tissue in either genotype, although again, there was a modest reduction in the respiration of BAT from *Prdm16*$^{lox/lox}$ mice (Figure 3G). Therefore, using two models of browning/beiging, these data demonstrate that creatine reduction attenuates the oxidative metabolism of thermogenic adipose tissues in vivo.

Respiration of Cultured Human Brown Adipocytes Is Regulated by Creatine

Much, though not all, of the brown fat observed in adult humans has characteristics of murine beige adipocytes (Lidell et al., 2013; Shinoda et al., 2015; Wu et al., 2012). Thus, it was of interest to examine whether creatine contributed to oxidative metabolism in the recently cloned human brown adipocytes (Shinoda et al., 2015). Both *Ckmt1* and *Ckmt2* mRNA levels were higher in two human clonal brown adipocyte lines compared to human white adipocytes (Figure 3H). When human brown adipocytes were treated with β-GPA, basal respiration was significantly reduced by 45%; this reduction was completely rescued by creatine supplementation (Figure 3I), demonstrating the specificity of β-GPA. Next, RNAi-mediated knockdown was used to assess the function of *Ckmt1* in these adipocytes. Transfection of small interfering RNAs (siRNAs) targeting *Ckmt1* resulted in an ~40% reduction in *Ckmt1* mRNA levels, relative to control siRNA-transfected cells (Figure S3D). Knockdown of *Ckmt1* resulted in a 26% reduction in basal respiration, and creatine supplementation did not rescue this effect (Figure 3J). These data demonstrate that creatine and CKMT1 regulate oxidative properties of isolated human brown adipocytes.

Compensatory Regulation of Creatine Metabolism Components and UCP1 in Adipose Tissues In Vivo

The ability of creatine to stimulate thermogenesis in an apparently sub-stoichiometric manner with respect to ADP-dependent respiration suggested that this creatine-based futile cycle could be an important mechanism of thermoregulation in vivo, independent of UCP1. To begin to test this supposition, we re-examined the longstanding and important observation that mice lacking *Ucp1* can maintain thermal homeostasis at 4°C if they are gradually acclimated to this temperature (Golozoubova et al., 2001). These data demonstrated that alternative thermogenic pathway(s) compensate for the lack of UCP1 (Ukropec et al., 2006). We therefore gradually acclimated *Ucp1*-deficient (*Ucp1*$^{-/-}$) mice to the cold over a period of 21 days. In addition, we also reduced creatine levels by administration of β-GPA to both *Ucp1*$^{+/+}$ and *Ucp1*$^{-/-}$ animals. As shown previously (Ukropec et al., 2006), cold-exposed *Ucp1*$^{-/-}$ mice had elevated expression of classical thermogenic genes, such as *Dio2* and *Pgc-1α*, in iWAT compared to *Ucp1*$^{+/+}$ mice (Figure 4A). *Pgc-1α* was also induced in BAT from *Ucp1*$^{-/-}$ mice (Figure S4A). These data suggest a strong induction of a thermogenic phenotype in the iWAT of *Ucp1*$^{-/-}$ mice. *Slc6a8* and *Ckmt1* transcripts were elevated in iWAT of cold-exposed *Ucp1*$^{-/-}$ mice, relative to *Ucp1*$^{+/+}$ littermates (Figure 4B), whereas *Slc6a8* and *Ckmt2* transcript levels were higher in BAT from the same animals (Figure S4B).

As the induction of creatine metabolism genes was elevated in *Ucp1*$^{-/-}$ mice, classical thermogenic genes, such as *Ucp1* and *Dio2*, were significantly elevated in iWAT of cold-exposed mice after creatine reduction with β-GPA (Figure 4C). A modest increase in *Ucp1* and *Pgc-1α* mRNA was observed in BAT of cold-exposed *Ucp1*$^{+/+}$ mice following creatine reduction with β-GPA (Figure S4C). UCP1 protein levels were also elevated in response to β-GPA in iWAT of *Ucp1*$^{+/+}$ mice but did not change in the BAT of the same animals (Figure 4D).

We also examined the compensatory regulation between creatine metabolism genes and Ucp1 in human brown adipocytes. In these cell lines, *Ckmt1* was more abundant than *Ckmt2* at the mRNA level (Figure 3H). Transfection of siRNAs targeting human *Ckmt1* resulted in an ~40% reduction in *Ckmt1* mRNA levels, relative to control siRNA-transfected cells (Figure 4E). Strikingly, *Ucp1* mRNA was elevated 2.5-fold in cells transfected with *Ckmt1*-targeted siRNAs relative to control siRNA-transfected cells. Forskolin treatment of human brown-fat cells resulted in a near 8-fold induction of *Ucp1* mRNA (Figure 4E), and combining forskolin treatment with *Ckmt1* knockdown resulted in a 15-fold elevation in *Ucp1* transcript abundance above non-treated si-Ctrl cells (Figure 4E). Furthermore, si-Ckmt1-transfected cells had an elevated abundance of *Dio2* and *Pgc-1α*, relative to si-Ctrl transfected cells, following forskolin treatment (Figure 4E). Taken together, these data demonstrate

Figure 3. Creatine Metabolism in Adipose Tissue Contributes to Energy Expenditure and Thermal Homeostasis In Vivo

(A) Creatine concentration in iWAT (beige), BAT, and gastrocnemius muscle (Gstrc) from cold-exposed C57BL/6 mice treated with four daily injections of vehicle or β-GPA (0.4 g kg^{-1}); n = 5 mice per group.

(B) Western blot of iWAT (beige) and BAT from animals treated as in (A); n = 3 mice per group.

(C) Movement, n = 8 mice per group. CL (0.2 mg kg^{-1}) was co-injected intraperitonealy with vehicle (saline) or β-GPA (0.4 g kg^{-1}).

(D) Food intake, n = 8 mice per group, treated as in (C).

(E) Oxygen consumption, n = 8 mice per group, treated as in (C).

(F) OCR of minced tissues following four daily injections of vehicle, β-GPA (0.4 g kg^{-1}), CL (0.2 mg kg^{-1}), or β-GPA + CL; n = 5 mice per group.

(G) OCR of minced tissues from *Prdm16*$^{lox/lox}$ and Adipo-PRDM16 KO mice after 7 days cold exposure. β-GPA was administered on the last 4 days of cold exposure; n = 5 to 7 mice per group.

(H) qRT-PCR of *Ckmt1* and *Ckmt2* in two human brown adipocyte lines (#11-1 and 11-3) and one human white adipocyte line (#11). Raw ct values are embedded in the bars.

(I) OCR of human brown adipocytes treated with vehicle, β-GPA (2 mM), and creatine (5 mM).

(J) OCR of human brown adipocytes transfected with si-Ctrl or si-Ckmt1. Creatine used at 5 mM.

Data are presented as means ± SEM. *p < 0.05, **p < 0.01, ***p < 0.0001.

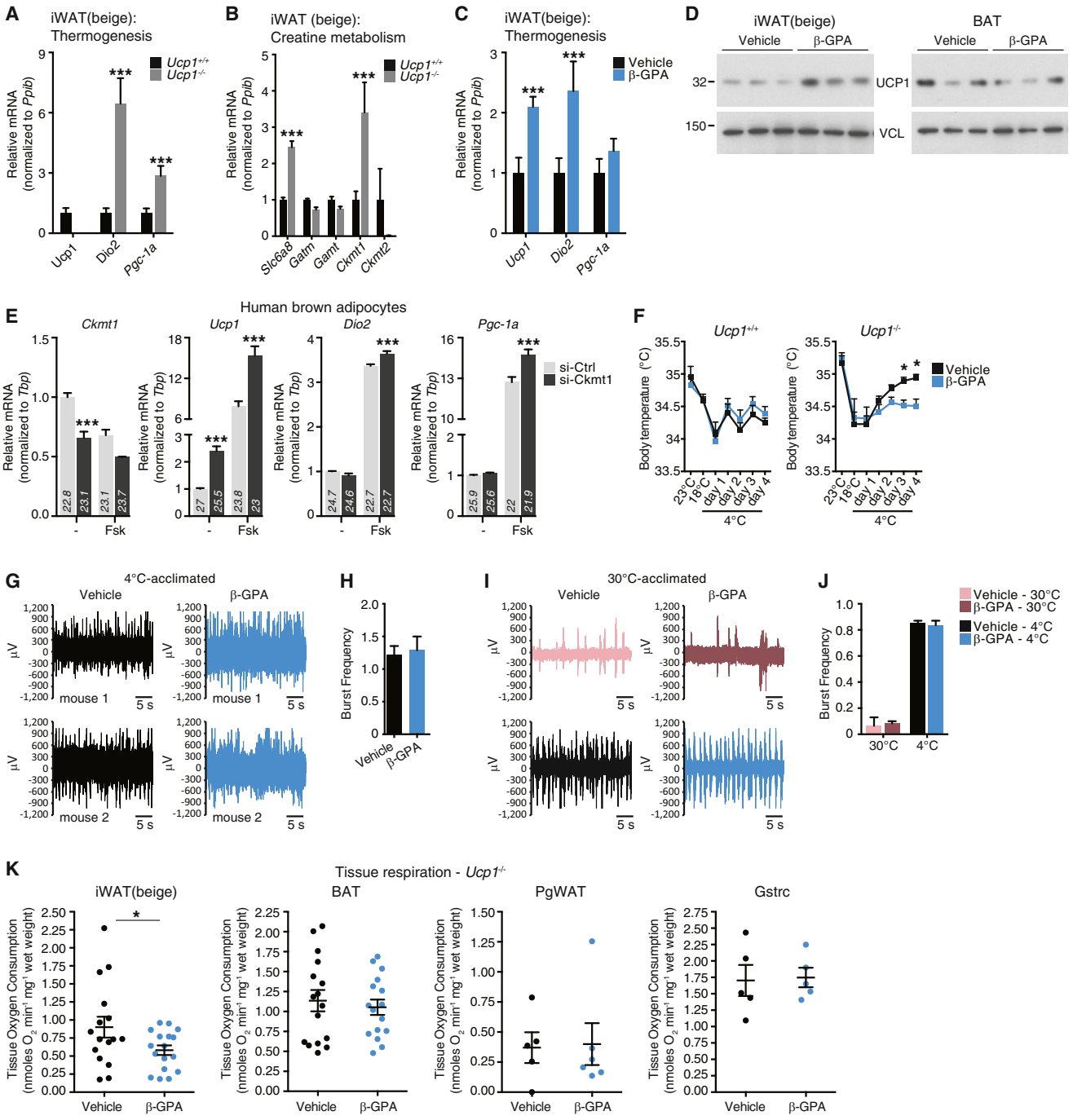

Figure 4. Creatine Metabolism Regulates UCP1-Independent Thermal Homeostasis In Vivo

(A) qRT-PCR from iWAT of 4°C-acclimated *Ucp1*$^{+/+}$ and *Ucp1*$^{-/-}$ mice; n = 5 mice per group.

(B) qRT-PCR of creatine metabolism genes from same samples as in (A).

(C) qRT-PCR from iWAT of 4°C-acclimated mice treated with four daily injections of vehicle or β-GPA (0.4 g kg^{-1}); n = 5 mice per group.

(D) Western blot from iWAT and BAT from mice treated as in (C). Vinculin (VCL), loading control, n = 3 mice per group.

(E) qRT-PCR of clonal human brown adipocytes (line #11-1). siRNAs targeted against control (si-Ctrl) or Ckmt1 (si-Ckmt1). Forskolin was used at 10 μM for 4 hr. (The data showing si-Ctrl and si-Ckmt1, without forskolin treatment, are the same data shown in Figure S3D); n = 3 per group.

(F) Body temperature of *Ucp1*$^{+/+}$ and *Ucp1*$^{-/-}$ mice treated with vehicle or β-GPA (0.4 g kg^{-1}); n = 7 to 8 mice per group.

(G) Representative electromyogram (EMG) traces, measured at 4°C, of 4°C-acclimated *Ucp1*$^{-/-}$ mice treated as in (F).

(H) Frequency of shivering bursts quantified from data in (G).

(I) Representative EMG traces, at 30°C and following 15–45 min at 4°C, of 30°C-acclimated wild-type C57BL/6 mice treated as in (F).

(legend continued on next page)

that genes involved in creatine metabolism are increased in the absence of UCP1, and expression of classical thermogenic genes is elevated when creatine metabolism is disrupted. These data suggest a compensatory relationship between UCP1- and creatine-dependent bioenergetics in mice and humans.

Creatine Regulates UCP1-Independent Thermal Homeostasis In Vivo

To test the role of creatine metabolism in adaptive thermogenesis in vivo, we examined the body temperature of cold-acclimated *Ucp1*$^{+/+}$ and *Ucp1*$^{-/-}$ mice that were treated with either β-GPA or vehicle for 4 days. *Ucp1*$^{-/-}$ mice weighed slightly less than *Ucp1*$^{+/+}$ mice (Figure S4D). Body temperature of *Ucp1*$^{-/-}$ mice was higher than that of *Ucp1*$^{+/+}$ animals at 23°C and 4°C (Figure 4F) (*Ucp1*$^{+/+}$: 34.4 ± 0.11°C and *Ucp1*$^{-/-}$: 34.7 ± 0.14°C, at 4°C). This temperature difference between genotypes is consistent with previous work (Liu et al., 2003). Strikingly, body temperature of the *Ucp1*$^{-/-}$ animals was significantly lower when endogenous creatine levels were reduced with β-GPA (Figure 4F), suggesting that in the absence of UCP1, creatine regulates a larger proportion of cold-induced thermogenesis than when UCP1 is present.

Creatine contributes to skeletal muscle metabolism, and so it was critical to determine whether the effect of β-GPA on body temperature was due to reductions in shivering thermogenesis. Thus, we used electromyography (EMG) to monitor shivering directly. Mice housed at 30°C showed minimal EMG activity. However, within 15 to 30 min of exposure to 4°C, bursts of shivering were detected (Figure S4E). Next, we used EMG on *Ucp1*$^{-/-}$ mice that had been acclimated to 4°C, and similar to previous work (Golozoubova et al., 2001), we detected robust shivering activity (Figure S4E). These measurements were confirmed as shivering bursts because they were abolished with the nicotinic acetylcholine receptor inhibitor D-tubocurarine (Figure S4E). The capacity for shivering of cold-acclimated *Ucp1*$^{-/-}$ mice was not altered by β-GPA treatment (Figures 4G and 4H). We next examined shivering thermogenesis and body temperature in wild-type mice that had been acclimated to 30°C and acutely cold challenged at 4°C following administration of vehicle or β-GPA for 4 days. Under these conditions, reduced creatine levels did not alter shivering capacity (Figures 4I and 4J) or body temperature (Figure S4F). Analysis of serum CK activity was used as an independent method to monitor shivering. Although serum CK activity was elevated in *Ucp1*$^{-/-}$ mice at 18°C, CK activity was elevated to a similar extent in *Ucp1*$^{+/+}$ and *Ucp1*$^{-/-}$ mice when ambient temperature was reduced to 10°C and 4°C (Figure S4G). Importantly, β-GPA administration had no effect on serum CK activity in either genotype. Together, these results indicate that the reduced body temperature of β-GPA-treated *Ucp1*$^{-/-}$ mice was not due to aberrant shivering, and that the metabolic and thermogenic adaptations that exist in the absence of UCP1 cannot be explained solely by shivering thermogenesis. Examination of respiration by isolated tissues indicated that despite a lower respiratory capacity of iWAT from *Ucp1*$^{-/-}$ mice, relative to *Ucp1*$^{+/+}$ mice (compare Figure 4K to Figure S4H), β-GPA treatment reduced oxygen consumption substantially in this depot from *Ucp1*$^{-/-}$ mice by 40% (Figure 4K). No significant effect on respiration due to creatine reduction was observed in any other tissue examined; however, a modest reduction was observed in BAT (Figures 4K and S4H).

A Screen of Mitochondrial Phosphatases to Identify Candidate Regulators of a Creatine-Driven Substrate Cycle

Taken together, our data indicated that creatine drives high-energy phosphate-dependent substrate cycling, which requires ADP-stimulated respiration. This led us to consider candidate molecules in adipose mitochondria that could carry out this process. To this end, we mined our mitochondrial proteomics inventory for putative phosphatases/hydrolases and identified 11 candidate phosphatases. Because several known members of creatine metabolism had elevated expression in *Ucp1*$^{-/-}$ mice (Figure 4B), we posited that the expression of a key enzyme(s) with phosphatase activity might also be elevated in the absence of UCP1. Transcript levels for all 11 of these phosphatases were measured in iWAT and BAT of cold-exposed *Ucp1*$^{+/+}$ and *Ucp1*$^{-/-}$ mice. One gene—*Phospho1* (phosphatase orphan 1)—was dramatically altered at the mRNA level, with an 8-fold increase in iWAT of *Ucp1*$^{-/-}$ animals (Figure 5A). In contrast, none of the candidates were increased in BAT at the mRNA level (Figure S5A). The consistent identification of PHOSPHO1 in our mitochondrial proteomic experiments suggested that PHOSHPO1 is at least partly associated with adipose mitochondria. Strikingly, protein expression of PHOSPHO1 was dramatically higher in the iWAT and BAT of *Ucp1*$^{-/-}$ mice, relative to *Ucp1*$^{+/+}$ mice (Figure 5B). PHOSPHO2, the closest homolog of PHOSPHO1, displayed the opposite expression pattern (Figure 5B). Proteomic quantification of PHOSPHO1 from iWAT and BAT of cold-acclimated *Ucp1*$^{+/+}$ and *Ucp1*$^{-/-}$ mice also demonstrated results similar to those of western blotting (Figure S5B). Interestingly, creatine reduction with β-GPA resulted in a small increase in *Phospho1* mRNA levels in iWAT from cold-exposed *Ucp1*$^{+/+}$ mice (Figure 5C), and a modest trend in the same direction was detected in BAT (Figure S5C). We also examined the compensatory regulation between Phospho1 and Ucp1 in human brown adipocytes. Transfection of siRNAs targeting human *Phospho1* resulted in an ~50% reduction in *Phospho1* mRNA levels, relative to control siRNA-transfected cells (Figure 5D). *Ucp1* mRNA was significantly elevated 1.5-fold in cells transfected with *Phospho1*-targeted siRNAs relative to control siRNA-transfected cells, and no change was observed for the differentiation marker *Pparg* (Figure 5D). Therefore, based on the reciprocal expression pattern between

(J) Frequency of shivering bursts quantified from data in (I).

(K) OCR of minced tissues from 4°C-acclimated *Ucp1*$^{-/-}$ mice treated as in (F). n = 16 to 17 mice per group (iWAT and BAT); n = 5 to 6 mice per group (PgWAT and Gstrc).

Data are presented as means ± SEM. *p < 0.05, ***p < 0.0001.

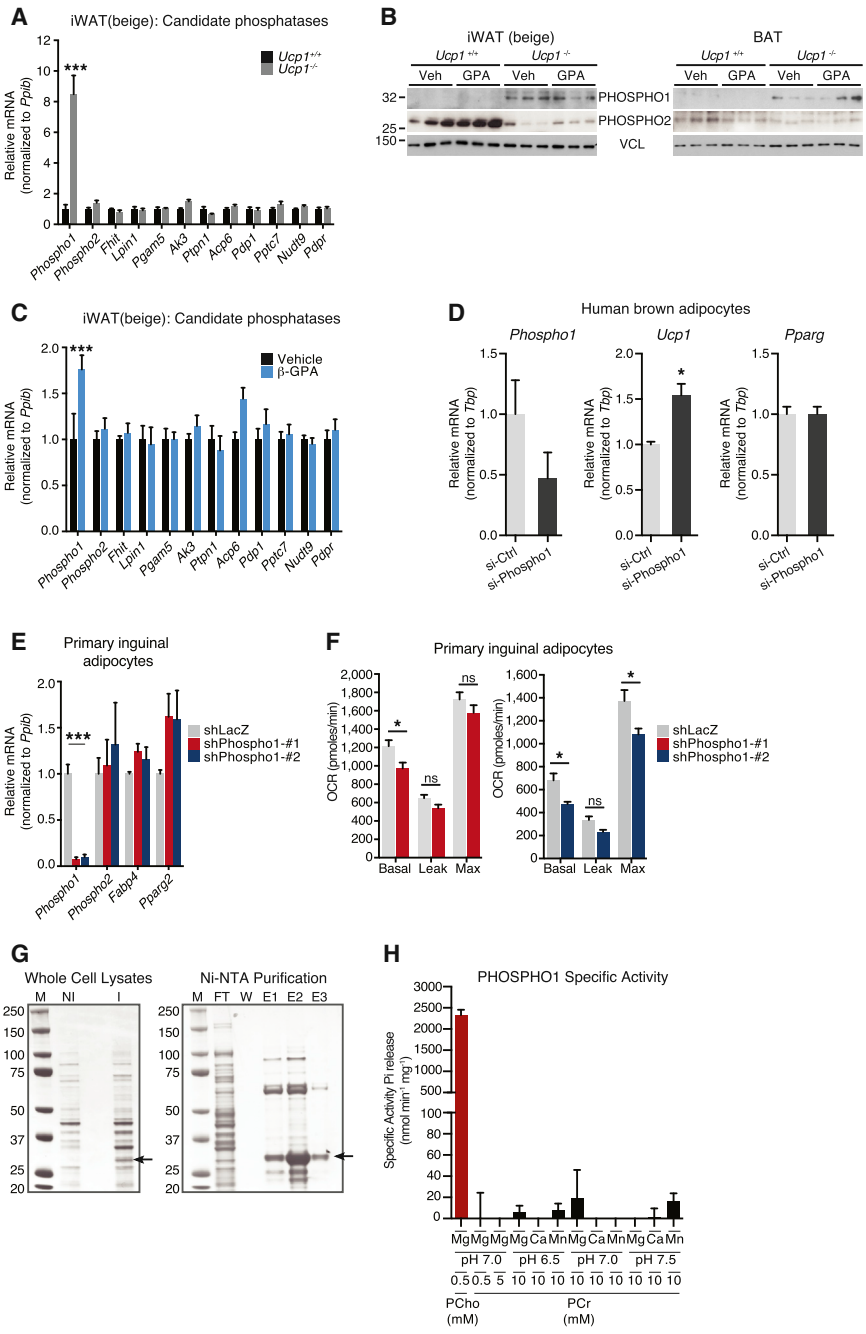

Figure 5. A Screen of Mitochondrial Phosphatases with *Ucp1*-Deficient Mice Identifies PHOSPHO1 as a Regulator of Adipocyte Respiration

(A) qRT-PCR of candidate phosphatases in iWAT of 4°C-acclimated *Ucp1*$^{+/+}$ and *Ucp1*$^{-/-}$ mice; n = 5 mice per group.

(B) Western blot of PHOSPHO1 and PHOSPHO2 from 4°C-acclimated *Ucp1*$^{+/+}$ and *Ucp1*$^{-/-}$ mice, treated with vehicle or β-GPA (0.4 g kg^{-1}). Vinculin (VCL), loading control.

(C) qRT-PCR of candidate phosphatases in iWAT of 4°C-acclimated wild-type mice treated as in (B); n = 5 mice per group.

(D) qRT-PCR of clonal human brown adipocytes (line #11-1) treated with si-Ctrl or si-Phospho1; n = 3 per group.

(E) qRT-PCR of primary mouse inguinal adipocytes after *Phospho1* knockdown (shPhospho1-#1 and shPhospho1-#2); n = 4 to 5 per group.

(F) OCR of primary mouse inguinal adipocytes treated as in (E); n = 5 to 7 per group.

(G) Coomassie stain of SDS-PAGE demonstrating PHOSPHO1 protein expression and purification. M, molecular weight marker; NI, non-induced; I, induced; FT, flow-through; W, wash; E1–E3, elutions 1–3. Arrows indicate recombinant PHOSPHO1.

(H) Specific activity of PHOSPHO1 toward PCho (0.5 mM) and PCr (0.5 to 10 mM) exposed to various buffer pH and divalent metals.

Data are presented as means ± SEM. *p < 0.05, ***p < 0.0001.

Phospho1 and *Ucp1* in mouse tissue and human cultured cells, PHOSPHO1 was considered as a candidate for involvement in a creatine-driven substrate cycle.

PHOSPHO1 Regulates Oxidative Metabolism in Primary Inguinal Adipocytes

Phospho1 displayed an expression pattern that would be predicted for a factor involved in an alternative, UCP1-independent pathway of energy expenditure. At the mRNA level, its steady-state expression was modestly higher in murine primary inguinal adipoyctes, relative to primary brown-fat cells, whereas *Ucp1* demonstrated the opposite expression pattern (Figure S5D). Therefore, the role of PHOSPHO1 in adipocyte bioenergetics was examined. Using adenoviral-mediated shRNA delivery, we achieved ~90% knockdown of *Phospho1* at the mRNA level in primary inguinal cells, with no mRNA changes detected for its homolog, *Phospho2*, or the differentiation markers *Fabp4* and *Pparg2* (Figure 5E). Reduced PHOSPHO1 levels were also observed at the protein level (Figure S5E). Both shRNAs used to knock down PHOSPHO1 significantly reduced basal oxygen consumption but had no effect on proton leak; the second shRNA also reduced maximal respiration (Figure 5F). Knockdown of *Phospho1* in primary brown adipocytes (Figure S5F) decreased basal respiration but had no effect on proton leak or maximal respiration (Figure S5G). Thus, reduced Phospho1 levels attenuated oxygen consumption in primary inguinal and brown adipocytes, although the relative effect was greater in inguinal cells. The more pronounced effect on basal respiration (largely regulated by ATP demand) than on proton leak is consistent with a role for PHOSPHO1 in

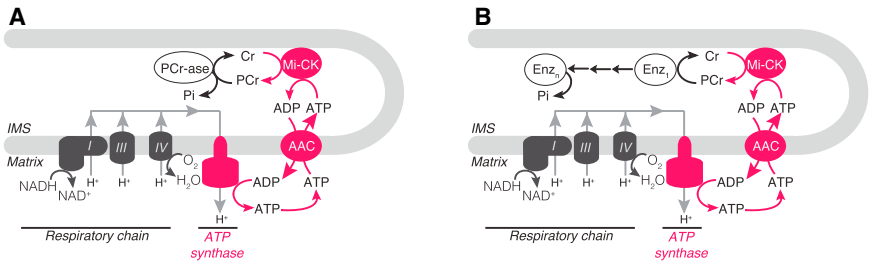

Figure 6. Models of Creatine-Driven Futile Substrate Cycling

(A) Model of creatine-driven futile substrate cycling based on direct hydrolysis of PCr.

(B) Model of creatine-driven futile substrate cycling based on multiple phosphotransfer events catalyzed by multiple enzymes (Enz_1–Enz_n).

ATP-coupled oxygen consumption. One interpretation of this data was that PHOSPHO1 regulates substrate cycling by liberating the high-energy phosphate from PCr. Therefore, we purified recombinant PHOSPHO1 (Figure 5G) in order to examine whether PCr can be directly hydrolyzed by PHOSPHO1 in vitro. PHOSPHO1-specific activity toward phosphocholine was similar to that of a prior report (Roberts et al., 2004). However, there was limited phosphatase activity toward PCr; this was done under various buffer conditions (Figure 5H). Taken together, these data suggest that if PHOSPHO1 is involved in a creatine-driven substrate cycle, it likely regulates high-energy phosphate metabolism downstream of the phosphotransfer event that utilizes PCr (Figure 6).

DISCUSSION

Although UCP1 is critical for optimal thermogenesis, *Ucp1*$^{-/-}$ animals can survive cold temperatures if gradually acclimated (Golozoubova et al., 2001; Meyer et al., 2010; Ukropec et al., 2006). Furthermore, it has been shown with adrenergic stimulation and peptide factors that the thermogenic responses of *Ucp1*$^{+/+}$ and *Ucp1*$^{-/-}$ mice are similar (Granneman et al., 2003; Grimpo et al., 2014; Véniant et al., 2015). These findings imply the presence of UCP1-independent thermogenic mechanisms. Glycerol-3-phosphate shuttle activation and lipid turnover (Flachs et al., 2011; Grimpo et al., 2014) have been posited to act independently of UCP1. Calcium cycling has been proposed to be an additional source of thermogenesis in BAT (Ukropec et al., 2006) and is a well-established thermogenic mechanism in the extraocular heater muscle cells of certain fish and in mammalian skeletal muscle (Bal et al., 2012; Block et al., 1994). Interestingly, large reductions in creatine levels have previously been linked to deregulated thermal homeostasis in rats (Wakatsuki et al., 1996; Yamashita et al., 1995), through unknown mechanisms.

The stoichiometric relationships observed between creatine, ADP, and oxygen consumption suggest a creatine-driven substrate cycle. By liberating a molar excess of ADP, with respect to the amount of added creatine, beige-fat mitochondria enhance respiration by maintaining a state of ATP synthesis, as shown by the increased rate of oxygen consumption when ADP was limiting. Reducing creatine levels by even 50% in beige and brown fat was associated with a blunted response to β3-agonism at the level of whole-body energy expenditure. A role for creatine and creatine kinase in brown adipose tissue metabolism has been posited previously (Berlet et al., 1976; Terblanche et al., 1998; Watanabe et al., 2008). Our data suggest that creatine metabolism regulates energy expenditure in both beige and brown fat.

Gene-expression analyses demonstrated a clear compensatory regulation between classical thermogenic genes and the genes involved in creatine metabolism in murine tissues and human adipocytes. Consistent with this reciprocal relationship, a reduction in creatine levels attenuated oxygen consumption of iWAT from *Ucp1*$^{-/-}$ mice and perturbed thermal homeostasis of these animals without diminishing shivering. The expression of *Phospho1* was elevated at the mRNA and protein level in *Ucp1*-deficient animals and thus became the focus of examination. Although the effect of PHOSPHO1 knockdown on adipocyte bioenergetics is consistent with a role for it in high-energy phosphate metabolism, PHOSPHO1 does not hydrolyze PCr in vitro, at least under any conditions we tested. Interestingly, phosphoethanolamine (PEtn), a direct PHOSPHO1 substrate (Roberts et al., 2004), has been demonstrated to inhibit ADP-stimulated mitochondrial respiration (Gohil et al., 2013), and so PHOSPHO1 could affect oxygen consumption by regulating PEtn levels.

The data presented here indicate that creatine metabolism plays an important role in adipose energy expenditure in vivo. Most likely, creatine facilitates the regeneration of ADP through futile hydrolysis of PCr. This could occur in a single enzymatic step, whereby PCr would be the direct substrate of a so-called PCr phosphatase (Figure 6A), or via multiple phosphotransfer reactions prior to phosphate hydrolysis from a currently unknown phosphometabolite (Figure 6B).

Similar to what was shown in the recently cloned human brown adipocytes (Shinoda et al., 2015), CKMT1 and CKMT2 expression is enriched in human BAT (Svensson et al., 2011). If creatine metabolism plays a substantial role in thermogenesis in humans, as suggested by the work here with isolated cells, it could open up possibilities to manipulate energy expenditure in patients with metabolic diseases by new drugs or even with dietary supplementation.

EXPERIMENTAL PROCEDURES

Sucrose Gradient-Purified Mitochondria

Sucrose was dissolved to a concentration of 1M and 1.5M in gradient buffer (10 mM HEPES, pH 7.8, 5 mM EDTA, and 2 mM DTT) and layered in a polyallomer centrifuge tube. Mitochondrial samples were loaded on top of the gradient and ultracentrifuged at 32,000 rpm for 1 hr at 4°C. Intact organelles that banded at the interface of the sucrose cushion were carefully extracted, washed twice in SHE buffer, and stored at −80°C until LC-MS/MS or western blot analyses.

Mitochondrial Respiration

Mitochondrial respiration was determined using an XF24 Extracellular Flux Analyzer (Seahorse Bioscience) using 15 μg mitochondrial protein in a buffer containing 50 mM KCl, 4 mM KH2PO4, 5 mM HEPES, and 1 mM EGTA, 4%

BSA, 10 mM pyruvate, 5 mM malate, 1 mM GDP. Mitochondria were plated and centrifuged 2,000 g for 20 min to promote adherence to the XF24 V7 cell-culture microplate. Uncoupled and maximal OCR was determined using oligomycin (14 μM) and FCCP (10 μM). Rotenone and antimycin A (4 μM each) were used to inhibit complex 1- and complex 3-dependent respiration.

Primary Inguinal Adipocyte Differentiation

Primary inguinal preadipocytes were counted and plated in the evening at 20,000 cells per well of a seahorse plate. The following morning, inguinal preadipocytes were induced to differentiate with 1 μM rosiglitazone, 0.5 mM isobutylmethylxanthine (IBMX), 1 μM dexamethasone, and 5 μg ml^{-1} insulin. Cells were re-fed every 48 hr with 1 μM rosiglitazone and 5 μg ml^{-1} insulin. Cells were fully differentiated by day 5 post-induction.

Primary Brown Adipocyte Differentiation

Primary brown preadipocytes were counted and plated in the evening at 15,000 cells per well of a seahorse plate. The following morning, brown preadipocytes were induced to differentiate with 1 μM rosiglitazone, 0.5 mM IBMX, 5 μM dexamethasone, 0.114 μg ml^{-1} insulin, 1 nM T3, and 125 μM indomethacin. Cells were re-fed every 48 hr with 1 μM rosiglitazone and 0.5 μg ml^{-1} insulin. Cells were fully differentiated by day 5 post-induction.

SUPPLEMENTAL INFORMATION

Supplemental Information includes Supplemental Experimental Procedures, five figures, and three tables and can be found with this article online at http://dx.doi.org/10.1016/j.cell.2015.09.035.

AUTHOR CONTRIBUTIONS

Conceptualization, L.K. and B.M.S.; Methodology, L.K., E.T.C., B.M.S.; Investigation, L.K., E.T.C., M.P.J., B.K.E., K.S., G.Z.L.; Resources, D.L.-B., P.C., R.V., S.C.H.; Writing – Original Draft, L.K., E.T.C., B.M.S.; Writing – Review & Editing, L.K., E.T.C., P.C., B.M.S.; Funding Acquisition, L.K., E.T.C., S.K., S.P.G., B.M.S.; Supervision, S.K., S.P.G., B.M.S.

ACKNOWLEDGMENTS

We are grateful to Marc W. Kirschner, Mike P. Murphy, Bé Wieringa, and members of the Spiegelman lab for helpful discussions. pBAD-TOPO-TA/hPhospho1 was a kind gift from Colin Farquharson. The Biophysical Instrumentation Facility (NSF-0070319) is acknowledged for help with DSC. This work was supported by a Canadian Institutes of Health Research postdoctoral fellowship to L.K., by a Human Frontier Science Program postdoctoral fellowship to E.T.C., and by an NIH grant (DK031405) and the JPB foundation to B.M.S.

Received: April 26, 2015
Revised: July 10, 2015
Accepted: September 8, 2015
Published: October 22, 2015

REFERENCES

Bal, N.C., Maurya, S.K., Sopariwala, D.H., Sahoo, S.K., Gupta, S.C., Shaikh, S.A., Pant, M., Rowland, L.A., Bombardier, E., Goonasekera, S.A., et al. (2012). Sarcolipin is a newly identified regulator of muscle-based thermogenesis in mammals. Nat. Med. *18*, 1575–1579.

Berlet, H.H., Bonsmann, I., and Birringer, H. (1976). Occurrence of free creatine, phosphocreatine and creatine phosphokinase in adipose tissue. Biochim. Biophys. Acta *437*, 166–174.

Block, B.A., O'Brien, J., and Meissner, G. (1994). Characterization of the sarcoplasmic reticulum proteins in the thermogenic muscles of fish. J. Cell Biol. *127*, 1275–1287.

Bloom, J.D., Dutia, M.D., Johnson, B.D., Wissner, A., Burns, M.G., Largis, E.E., Dolan, J.A., and Claus, T.H. (1992). Disodium (R,R)-5-[2-[[2-(3-chlorophenyl)-2-hydroxyethyl]-amino] propyl]-1,3-benzodioxole-2,2-dicarboxylate (CL 316,243). A potent beta-adrenergic agonist virtually specific for beta 3 receptors. A promising antidiabetic and antiobesity agent. J. Med. Chem. *35*, 3081–3084.

Cannon, B., and Nedergaard, J. (2004). Brown adipose tissue: function and physiological significance. Physiol. Rev. *84*, 277–359.

Cohen, P., Levy, J.D., Zhang, Y., Frontini, A., Kolodin, D.P., Svensson, K.J., Lo, J.C., Zeng, X., Ye, L., Khandekar, M.J., et al. (2014). Ablation of PRDM16 and beige adipose causes metabolic dysfunction and a subcutaneous to visceral fat switch. Cell *156*, 304–316.

Feldmann, H.M., Golozoubova, V., Cannon, B., and Nedergaard, J. (2009). UCP1 ablation induces obesity and abolishes diet-induced thermogenesis in mice exempt from thermal stress by living at thermoneutrality. Cell Metab. *9*, 203–209.

Fitch, C.D., and Chevli, R. (1980). Inhibition of creatine and phosphocreatine accumulation in skeletal muscle and heart. Metabolism *29*, 686–690.

Flachs, P., Rühl, R., Hensler, M., Janovska, P., Zouhar, P., Kus, V., Macek Jilkova, Z., Papp, E., Kuda, O., Svobodova, M., et al. (2011). Synergistic induction of lipid catabolism and anti-inflammatory lipids in white fat of dietary obese mice in response to calorie restriction and n-3 fatty acids. Diabetologia *54*, 2626–2638.

Gohil, V.M., Zhu, L., Baker, C.D., Cracan, V., Yaseen, A., Jain, M., Clish, C.B., Brookes, P.S., Bakovic, M., and Mootha, V.K. (2013). Meclizine inhibits mitochondrial respiration through direct targeting of cytosolic phosphoethanolamine metabolism. J. Biol. Chem. *288*, 35387–35395.

Golozoubova, V., Hohtola, E., Matthias, A., Jacobsson, A., Cannon, B., and Nedergaard, J. (2001). Only UCP1 can mediate adaptive nonshivering thermogenesis in the cold. FASEB J. *15*, 2048–2050.

Granneman, J.G., Burnazi, M., Zhu, Z., and Schwamb, L.A. (2003). White adipose tissue contributes to UCP1-independent thermogenesis. Am. J. Physiol. Endocrinol. Metab. *285*, E1230–E1236.

Grimpo, K., Völker, M.N., Heppe, E.N., Braun, S., Heverhagen, J.T., and Heldmaier, G. (2014). Brown adipose tissue dynamics in wild-type and UCP1-knockout mice: in vivo insights with magnetic resonance. J. Lipid Res. *55*, 398–409.

Jacobus, W.E., and Lehninger, A.L. (1973). Creatine kinase of rat heart mitochondria. Coupling of creatine phosphorylation to electron transport. J. Biol. Chem. *248*, 4803–4810.

Lidell, M.E., Betz, M.J., Dahlqvist Leinhard, O., Heglind, M., Elander, L., Slawik, M., Mussack, T., Nilsson, D., Romu, T., Nuutila, P., et al. (2013). Evidence for two types of brown adipose tissue in humans. Nat. Med. *19*, 631–634.

Liu, X., Rossmeisl, M., McClaine, J., Riachi, M., Harper, M.E., and Kozak, L.P. (2003). Paradoxical resistance to diet-induced obesity in UCP1-deficient mice. J. Clin. Invest. *111*, 399–407.

Lowell, B.B., S-Susulic, V., Hamann, A., Lawitts, J.A., Himms-Hagen, J., Boyer, B.B., Kozak, L.P., and Flier, J.S. (1993). Development of obesity in transgenic mice after genetic ablation of brown adipose tissue. Nature *366*, 740–742.

Meyer, C.W., Willershäuser, M., Jastroch, M., Rourke, B.C., Fromme, T., Oelkrug, R., Heldmaier, G., and Klingenspor, M. (2010). Adaptive thermogenesis and thermal conductance in wild-type and UCP1-KO mice. Am. J. Physiol. Regul. Integr. Comp. Physiol. *299*, R1396–R1406.

Oudman, I., Clark, J.F., and Brewster, L.M. (2013). The effect of the creatine analogue beta-guanidinopropionic acid on energy metabolism: a systematic review. PLoS ONE *8*, e52879.

Ricquier, D., Gaillard, J.L., and Turc, J.M. (1979). Microcalorimetry of isolated mitochondria from brown adipose tissue. Effect of guanosine-di-phosphate. FEBS Lett. *99*, 203–206.

Roberts, S.J., Stewart, A.J., Sadler, P.J., and Farquharson, C. (2004). Human PHOSPHO1 exhibits high specific phosphoethanolamine and phosphocholine phosphatase activities. Biochem. J. *382*, 59–65.

Seale, P., Bjork, B., Yang, W., Kajimura, S., Chin, S., Kuang, S., Scimè, A., Devarakonda, S., Conroe, H.M., Erdjument-Bromage, H., et al. (2008). PRDM16 controls a brown fat/skeletal muscle switch. Nature *454*, 961–967.

Shabalina, I.G., Petrovic, N., de Jong, J.M., Kalinovich, A.V., Cannon, B., and Nedergaard, J. (2013). UCP1 in brite/beige adipose tissue mitochondria is functionally thermogenic. Cell Rep. *5*, 1196–1203.

Shinoda, K., Luijten, I.H., Hasegawa, Y., Hong, H., Sonne, S.B., Kim, M., Xue, R., Chondronikola, M., Cypess, A.M., Tseng, Y.H., et al. (2015). Genetic and functional characterization of clonally derived adult human brown adipocytes. Nat. Med. *21*, 389–394.

Sipilä, I. (1980). Inhibition of arginine-glycine amidinotransferase by ornithine. A possible mechanism for the muscular and chorioretinal atrophies in gyrate atrophy of the choroid and retina with hyperornithinemia. Biochim. Biophys. Acta *613*, 79–84.

Svensson, P.A., Jernås, M., Sjöholm, K., Hoffmann, J.M., Nilsson, B.E., Hansson, M., and Carlsson, L.M. (2011). Gene expression in human brown adipose tissue. Int. J. Mol. Med. *27*, 227–232.

Terblanche, S.E., Masondo, T.C., and Nel, W. (1998). Effects of cold acclimation on the activity levels of creatine kinase, lactate dehydrogenase and lactate dehydrogenase isoenzymes in various tissues of the rat. Cell Biol. Internat. *22*, 701–707.

Ukropec, J., Anunciado, R.P., Ravussin, Y., Hulver, M.W., and Kozak, L.P. (2006). UCP1-independent thermogenesis in white adipose tissue of cold-acclimated Ucp1-/- mice. J. Biol. Chem. *281*, 31894–31908.

Véniant, M.M., Sivits, G., Helmering, J., Komorowski, R., Lee, J., Fan, W., Moyer, C., and Lloyd, D.J. (2015). Pharmacologic effects of FGF21 are independent of the "browning" of white adipose tissue. Cell Metab. *21*, 731–738.

Wakatsuki, T., Hirata, F., Ohno, H., Yamamoto, M., Sato, Y., and Ohira, Y. (1996). Thermogenic responses to high-energy phosphate contents and/or hindlimb suspension in rats. Jpn. J. Physiol. *46*, 171–175.

Watanabe, M., Yamamoto, T., Kakuhata, R., Okada, N., Kajimoto, K., Yamazaki, N., Kataoka, M., Baba, Y., Tamaki, T., and Shinohara, Y. (2008). Synchronized changes in transcript levels of genes activating cold exposure-induced thermogenesis in brown adipose tissue of experimental animals. Biochim. Biophysic. Acta *1777*, 104–112.

Watt, I.N., Montgomery, M.G., Runswick, M.J., Leslie, A.G., and Walker, J.E. (2010). Bioenergetic cost of making an adenosine triphosphate molecule in animal mitochondria. Proc. Natl. Acad. Sci. USA *107*, 16823–16827.

Wu, J., Boström, P., Sparks, L.M., Ye, L., Choi, J.H., Giang, A.H., Khandekar, M., Virtanen, K.A., Nuutila, P., Schaart, G., et al. (2012). Beige adipocytes are a distinct type of thermogenic fat cell in mouse and human. Cell *150*, 366–376.

Wyss, M., and Kaddurah-Daouk, R. (2000). Creatine and creatinine metabolism. Physiol. Rev. *80*, 1107–1213.

Yamashita, H., Ohira, Y., Wakatsuki, T., Yamamoto, M., Kizaki, T., Oh-ishi, S., and Ohno, H. (1995). Increased growth of brown adipose tissue but its reduced thermogenic activity in creatine-depleted rats fed beta-guanidinopropionic acid. Biochim. Biophys. Acta *1230*, 69–73.

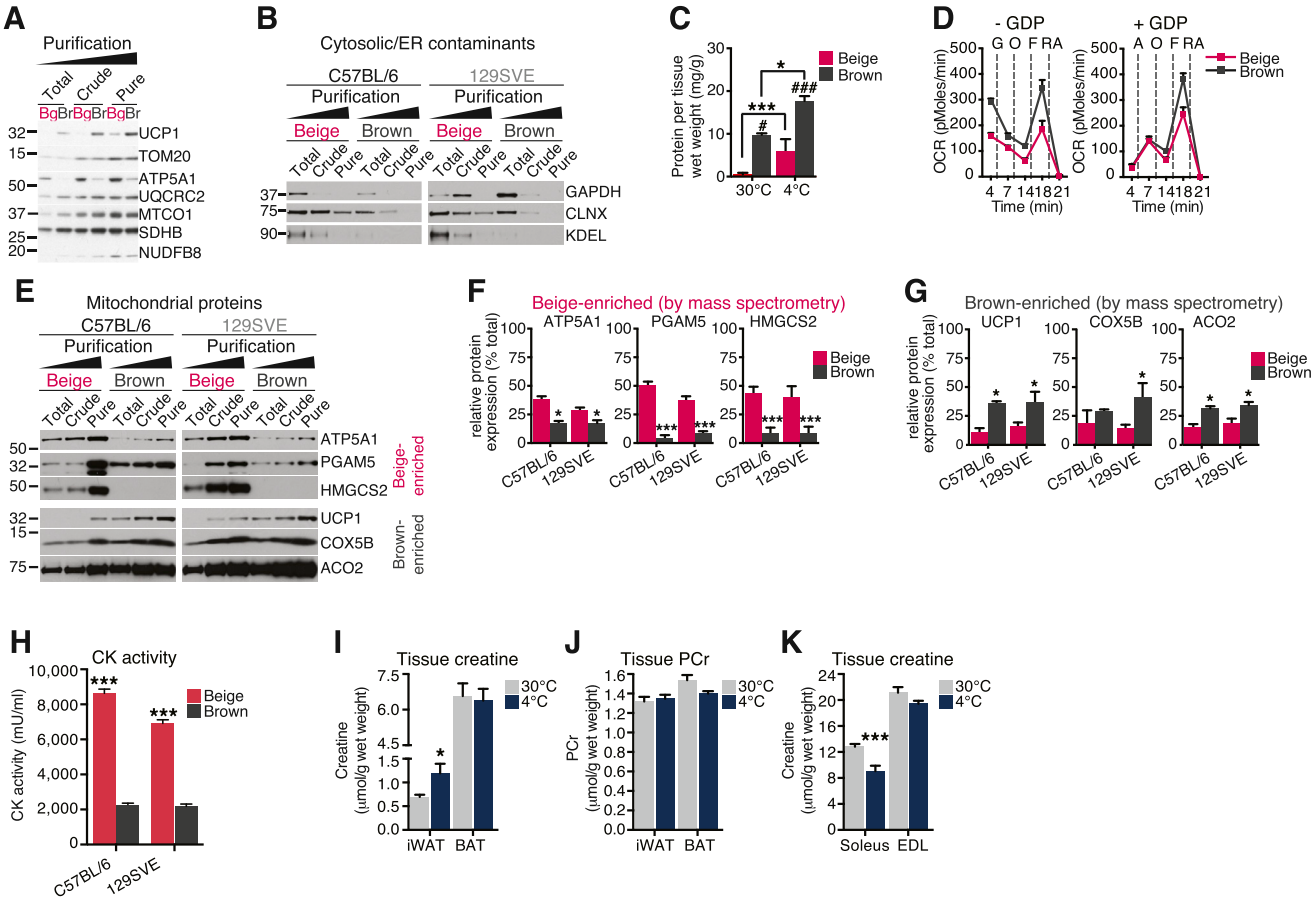

Figure S1. Characterization of Mitochondria from Cold-Exposed Brown and Beige Adipose Tissues, Related to Figure 1

(A) Western blot of mitochondrial proteins from whole tissue lysates (Total), crude mitochondria purified by differential centrifugation (Crude), and mitochondria purified on a sucrose gradient (Pure). 129SVE mice were cold-exposed (4°C) for one week. Beige-fat mitochondria (Bg), and brown-fat mitochondria (Br).

(B) Western blot of cytosolic (GAPDH) and endoplasmic reticulum (ER) (CLNX and KDEL) proteins from whole tissue lysates (Total), crude mitochondria purified by differential centrifugation (Crude), and mitochondria purified on a sucrose gradient (Pure). Mice were cold-exposed (4°C) for one week.

(C) Yield of beige and brown adipose mitochondria from 129SVE mice acclimated to thermoneutral (30°C) or cold (4°C) temperature. *$p < 0.05$ and ***$p < 0.01$, comparison of temperature. #$p < 0.05$ and ###$p < 0.01$, comparison of tissue.

(D) Oxygen consumption rate (OCR) of beige- and brown-fat mitochondria isolated from 129SVE mice, respiring on pyruvate/malate. Mitochondria (5 µg) were incubated in buffer without GDP (-GDP) or with GDP (+GDP), followed by the addition of the following compounds: 1 mM GDP (G), 1 mM ADP (A), 14 µM Oligomycin (O), 10 µM FCCP (F), and 4 µM each of rotenone/antimycin (RA).

(E) Western blot of beige- and brown-fat-enriched mitochondrial proteins from whole-tissue lysates (Total), crude mitochondria purified by differential centrifugation (Crude), and mitochondria purified on a sucrose gradient (Pure).

(F) Quantification of western blots, by densitometry, of mitochondrial proteins (ATP5A1, PGAM5, HMGCS2) that were identified as beige selective by proteomics. The signal intensity from beige- and brown-fat mitochondria from C57BL/6 and 129SVE mice was plotted as a percentage of the total sum (set to 100%) of all the intensities combined.

(G) Quantification of western blots, by densitometry, of mitochondrial proteins (UCP1, COX5B, ACO2) that were identified as brown-selective by proteomics. The signal intensity from beige- and brown-fat mitochondria from C57BL/6 and 129SVE mice was plotted as a percentage of the total sum (set to 100%) of all the intensities combined.

(H) CK activity of beige- and brown-fat mitochondria from cold-exposed (4°C) C57BL/6 and 129SVE mice.

(I) Creatine concentration in iWAT and BAT from mice (129SVE) housed at 30°C or seven days at 4°C; n = 6 mice per group.

(J) Phosphocreatine (PCr) concentration in iWAT and BAT from mice (129SVE) housed at 30°C or seven days at 4°C; n = 6 mice per group.

(K) Creatine concentration in soleus and extensor digitorum longus (EDL) from mice (129SVE) housed at 30°C or seven days at 4°C; n = 6 mice per group.

Data are presented as means ± SEM. *$p < 0.05$, ***$p < 0.01$.

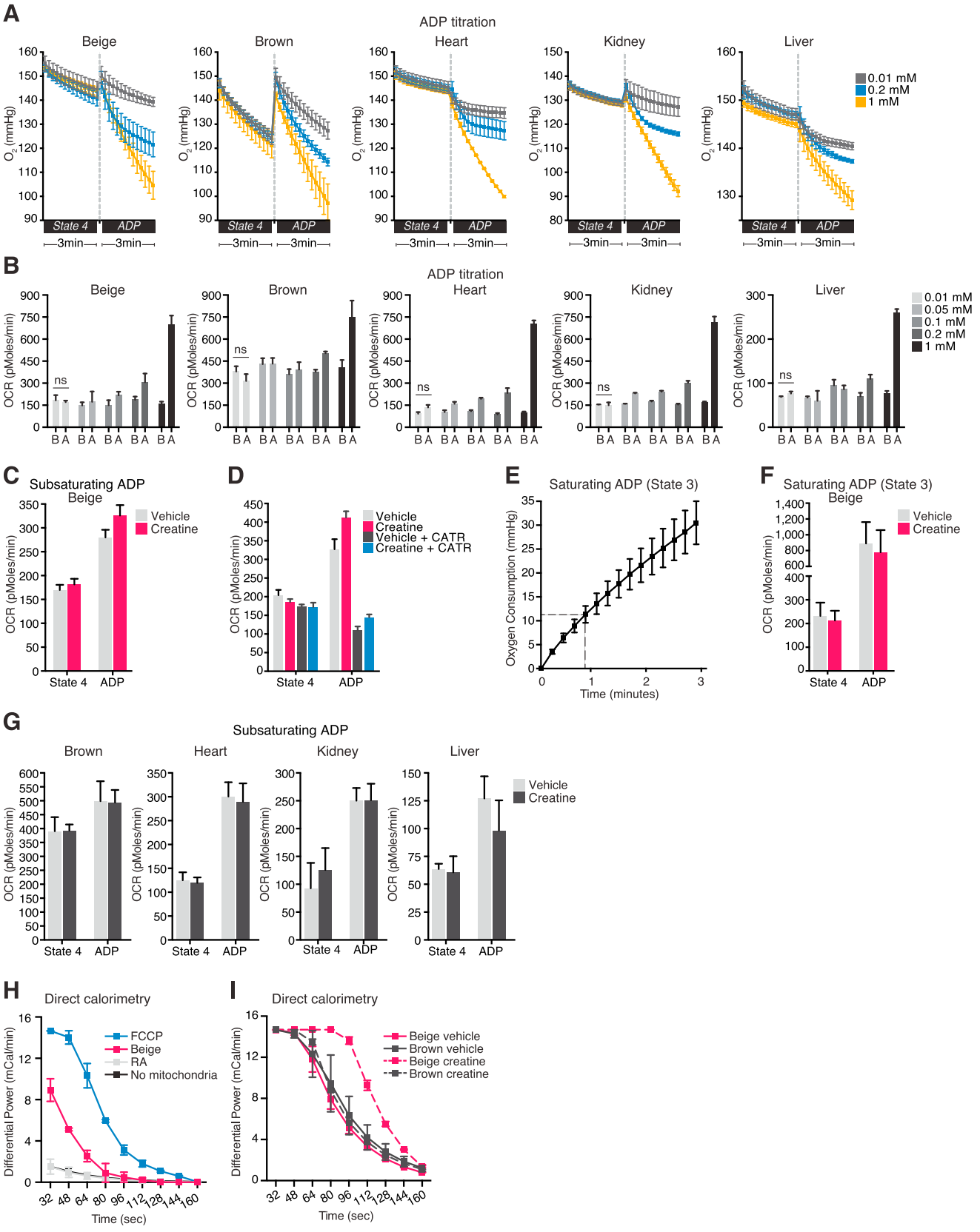

(legend on next page)

Figure S2. Creatine Stimulates Respiration in Beige-Fat Mitochondria when ADP Is Limiting, Related to Figure 2

(A) Oxygen consumption by beige fat, brown fat, heart, kidney, and liver mitochondria respiring on pyruvate/malate during state 4 respiration and following the addition of various concentrations of ADP (0.01, 0.2, and 1 mM). Mitochondria were isolated from C57BL/6 mice. Transition back to state 4 after ADP addition occurred ~48 s after stimulation with 0.2 mM ADP.

(B) Oxygen consumption rate (OCR) of beige fat, brown fat, heart, kidney, and liver mitochondria respiring on pyruvate/malate during basal state 4 (B) respiration or following the addition of various concentrations of ADP.

(C) OCR of beige-fat mitochondria (from C57BL/6 mice) incubated with or without creatine (0.01 mM) and respiring on pyruvate/malate during state 4 respiration or following the addition of ADP (0.2 mM).

(D) OCR of beige-fat mitochondria (from C57BL/6 mice) incubated with or without creatine (0.01 mM) and respiring on pyruvate/malate during state 4 respiration or following the addition of ADP (0.2 mM). Carboxyatractyloside (CATR) (10 μM) was used to inhibit the AAC.

(E) Oxygen consumption by beige-fat mitochondria following the addition of 1 mM ADP; n = 2 mitochondrial preparations, 15 mice per cohort.

(F) OCR of beige-fat mitochondria (from C57BL/6 mice) incubated with or without creatine (0.01 mM) and respiring on pyruvate/malate during state 4 respiration or following the addition of ADP (1 mM); n = 2 mitochondrial preparations, 15 mice per cohort.

(G) OCR of brown fat, heart, kidney, and liver mitochondria (from C57BL/6 mice) incubated with or without creatine (0.01 mM) and respiring on pyruvate/malate during state 4 respiration or following the addition of ADP (0.2 mM); n = 3 mitochondrial preparations, 15 mice per cohort.

(H) Differential power measured by differential scanning calorimetry (DSC) of beige-fat mitochondria (from 129SVE mice) respiring on of pyruvate/malate and treated with 10 μM FCCP to elicit maximal thermogenesis and 4 μM rotenone and antimycin A each (RA) to inhibit respiration; n = 2 mitochondrial preparations, 15 mice per cohort.

(I) Differential power measured by differential scanning calorimetry (DSC) of beige- and brown-fat mitochondria treated with vehicle or creatine (0.01 mM) in the presence of ADP. Mitochondrial respiration (state 4) was initiated with pyruvate/malate. Mitochondria were treated with ADP alone or with a combination of ADP and creatine. Samples were analyzed cross-sectionally; n = 2 mitochondrial preparations, 15 mice per cohort.

Data are presented as means ± SEM. *$p < 0.05$, ***$p < 0.01$.

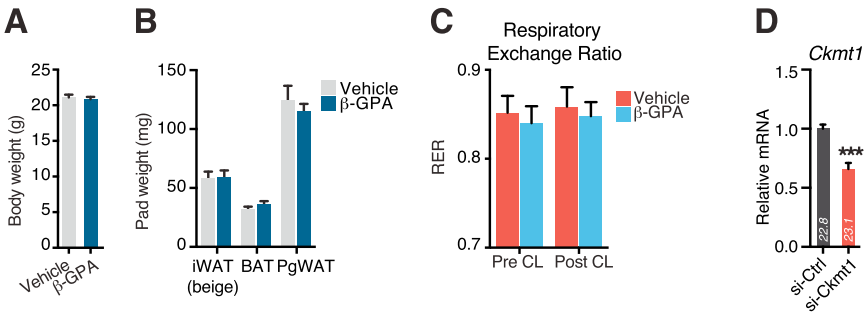

Figure S3. Creatine Bioenergetics in Adipose Tissue Contributes to Energy Expenditure and Thermal Homeostasis In Vivo, Related to Figure 3

(A) Body weight of C57BL/6 mice injected daily intraperitonealy with vehicle (saline) or β-GPA (0.4 g kg^{-1}) for 4 days; n = 7–8 mice per group.

(B) Tissue weights of iWAT, BAT, and PgWAT from C57BL/6 mice injected daily intraperitonealy with vehicle (saline) or β-GPA (0.4 g kg^{-1}) for 4 days; n = 7–8 mice per group.

(C) Respiratory exchange ratio (RER) for 6 hr before CL 316,243 injection (Pre CL) and 6 hr after CL 316,243 injection (Post CL) in C57BL/6 mice (n = 8 mice per group) co-injected intraperitonealy with vehicle (saline) or β-GPA (0.4 g kg^{-1}).

(D) Quantitative RT-PCR (qRT-PCR) of fully differentiated clonal human brown adipocytes, (line #11-1). siRNAs were targeted against control (si-Ctrl) or Ckmt1 (si-Ckmt1). Values are expressed relative to si-Ctrl cells, set to 1; n = 3 per group. (The data in D are the same data that are shown in the si-Ctrl- and si-Ckmt1-treated cells, without forskolin treatment, shown in Figure 4E).

Data are presented as means ± SEM. ***$p < 0.01$.

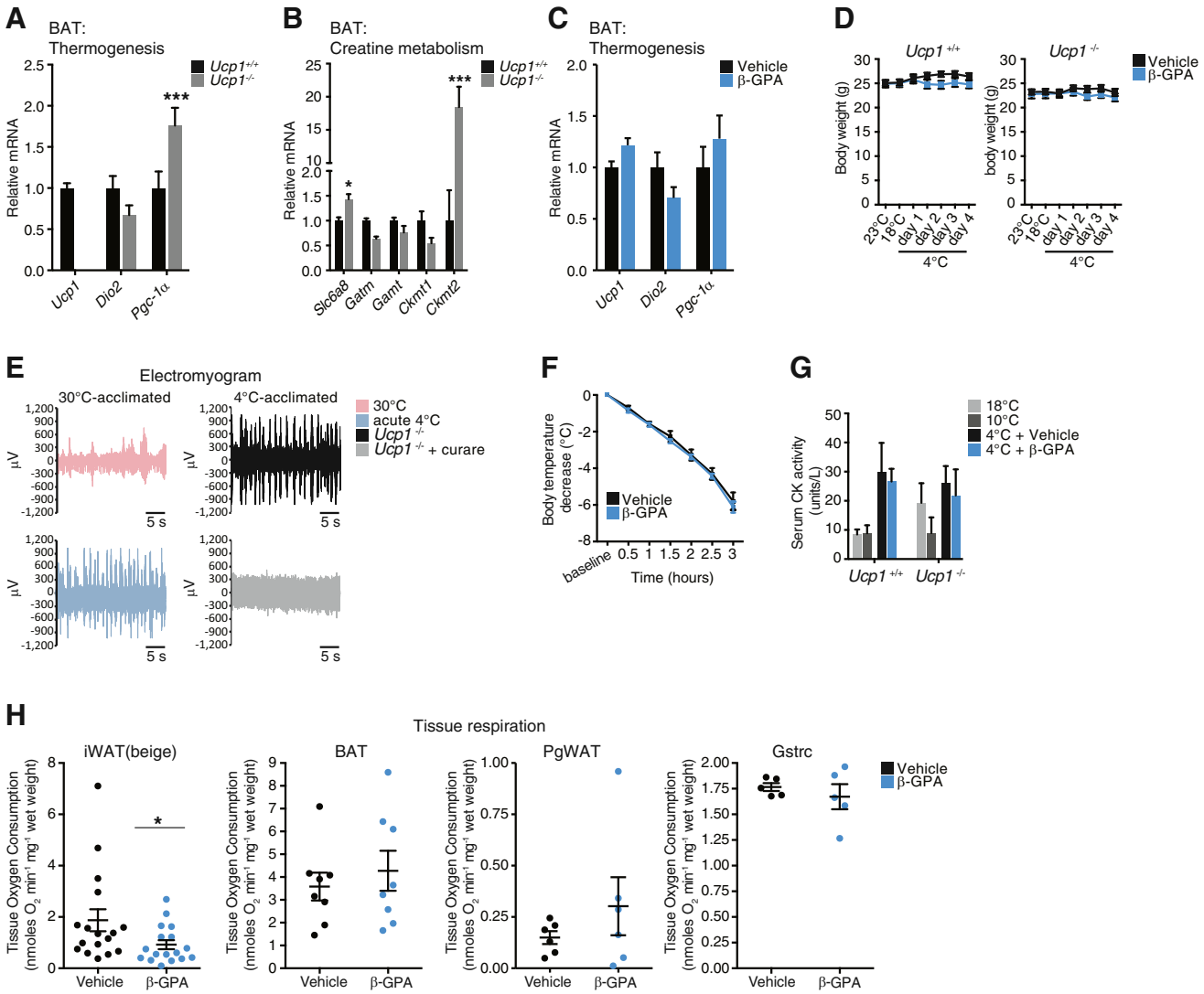

Figure S4. Creatine Metabolism Regulates UCP1-Independent Thermal Homeostasis In Vivo, Related to Figure 4

(A) qRT-PCR of classic thermogenic genes in BAT of 4°C-acclimated *Ucp1*$^{+/+}$ and *Ucp1*$^{-/-}$ mice; n = 5 mice per group.

(B) qRT-PCR of genes involved in creatine metabolism in BAT of 4°C-acclimated *Ucp1*$^{+/+}$ and *Ucp1*$^{-/-}$ mice; n = 5 mice per group.

(C) qRT-PCR of classic thermogenic genes in BAT of 4°C-acclimated mice treated with four daily injections of vehicle or β-GPA (0.4 g kg^{-1}); n = 5 mice per group.

(D) Body weight of *Ucp1*$^{+/+}$ and *Ucp1*$^{-/-}$ mice treated with four daily injections of vehicle or β-GPA (0.4 g kg^{-1}); n = 7 to 8 mice per group.

(E) Representative EMG of 30°C-acclimated wild-type female C57BL/6 mice exposed to 30°C (pink trace) or acute 4°C (blue trace), and EMG traces of 4°C-acclimated *Ucp1*$^{-/-}$ female mice exposed to 4°C and injected with vehicle (black trace) or 0.3 mg/kg curare (gray trace).

(F) Rectal temperature of C57BL/6 mice exposed acutely to 4°C after being housed at 30°C and treated with four daily injections of vehicle or β-GPA (0.4 g kg^{-1}); n = 5 mice per group.

(G) Serum CK activity of *Ucp1*$^{+/+}$ and *Ucp1*$^{-/-}$ mice after acclimation at various ambient temperatures, and then after treated with four daily injections of vehicle or β-GPA (0.4 g kg^{-1}) at 4°C; n = 7 to 8 mice per group.

(H) OCR of minced iWAT (beige), BAT, PgWAT, and Gstrc from 4°C-acclimated *Ucp1*$^{+/+}$ mice following four daily injections of vehicle or β-GPA (0.4 g kg^{-1}); n = 16 to 17 mice per group (iWAT and BAT); n = 5 to 6 mice per group (PgWAT and Gstrc).

Data are presented as means ± SEM. *p < 0.05, ***p < 0.01.

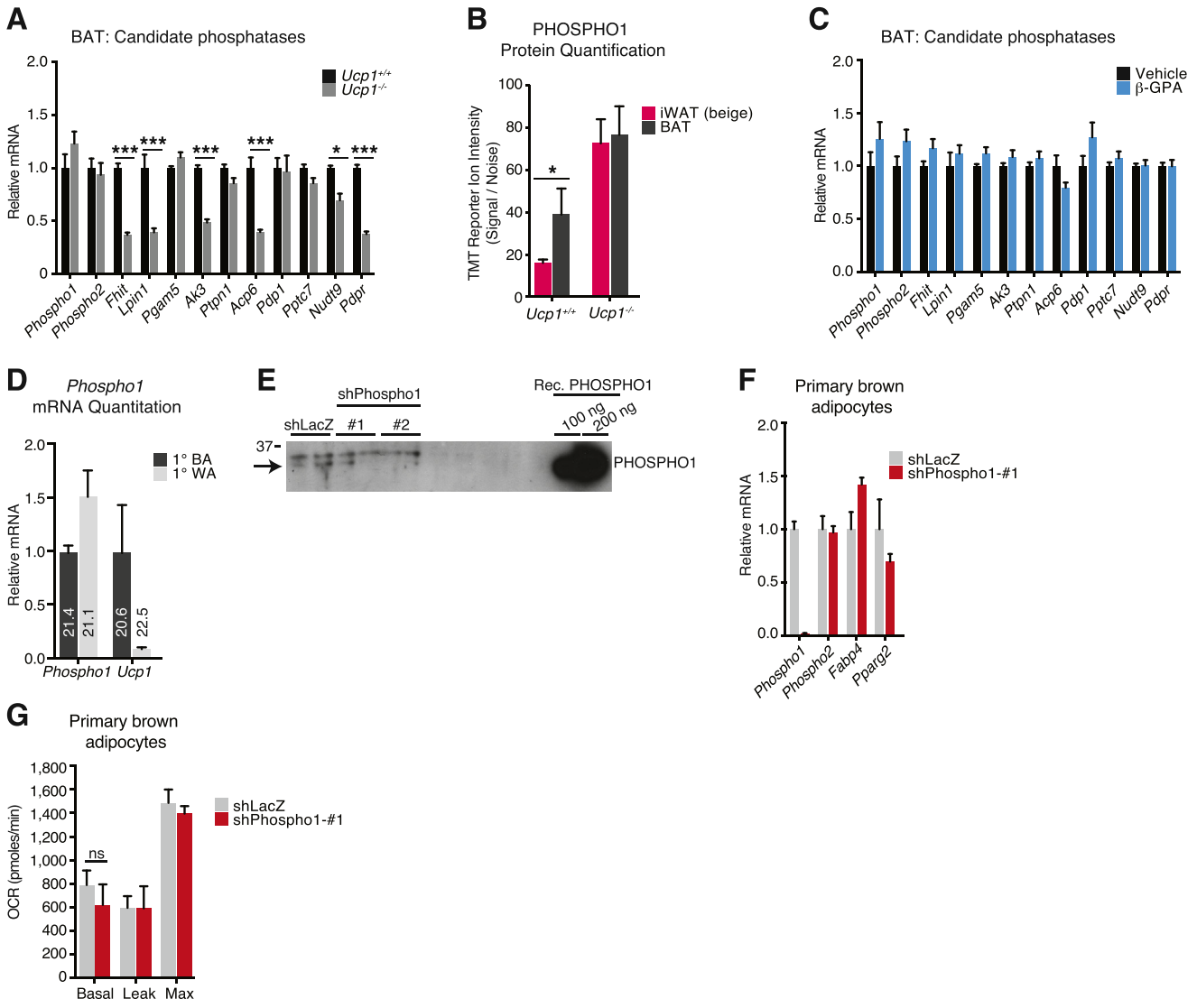

Figure S5. A Screen of Mitochondrial Phosphatases with *Ucp1*-Deficient Mice Identifies PHOSPHO1 as a Regulator of Adipocyte Respiration, Related to Figure 5

(A) qRT-PCR of candidate phosphatase genes in BAT of 4°C-acclimated *Ucp1*$^{+/+}$ and *Ucp1*$^{-/-}$ mice; n = 5 mice per group.

(B) PHOSPHO1 protein quantification in iWAT and BAT of 4°C-acclimated *Ucp1*$^{+/+}$ and *Ucp1*$^{-/-}$ mice by isobaric tagging.

(C) qRT-PCR of candidate phosphatase genes in BAT of 4°C-acclimated wild-type C57BL/6 mice treated with vehicle or β-GPA (0.4 g kg^{-1}); n = 5 mice per group.

(D) qRT-PCR of *Phospho1* and *Ucp1* from primary inguinal white adipocytes (WA) and primary brown adipocytes (BA), n = 4 to 5 per group. Raw ct values are embedded in the bar graph.

(E) Western blot of primary inguinal adipocyte lysates following knockdown of *Phospho1* with two shRNAs (shPhospho1-#1 and -#2), relative to shRNA targeted against *LacZ* (shLacZ). Recombinant PHOSPHO1 (Rec. PHOSPHO1) protein was loaded as an antibody control.

(F) qRT-PCR after adenoviral-mediated knockdown of *Phospho1* using shPhospho1-#1 in primary brown adipocytes; n = 3 to 4.

(G) OCR of primary mouse brown adipocytes transduced with shLacZ, or shPhospho1-#1; n = 5 to 7 per group. Leak respiration was examined with oligomycin (3 μM), and maximal respiration was examined with FCCP (1.8 μM).

Data are presented as means ± SEM. *p < 0.05, ***p < 0.01.

Cell

Supplemental Information

A Creatine-Driven Substrate Cycle Enhances Energy Expenditure and Thermogenesis in Beige Fat

Lawrence Kazak, Edward T. Chouchani, Mark P. Jedrychowski, Brian K. Erickson, Kosaku Shinoda, Paul Cohen, Ramalingam Vetrivelan, Gina Z. Lu, Dina Laznik-Bogoslavski, Sebastian C. Hasenfuss, Shingo Kajimura, Steve P. Gygi, and Bruce M. Spiegelman

SUPPLEMENTAL INFORMATION

SUPPLEMENTAL EXPERIMENTAL PROCEDURES

Animals

Mice were housed at 23°C under a 12 hr light/dark cycle with free access to food and water. All experiments used matched littermates. The breeding schemes for Adipo-PRDM16 KO and *Ucp1*$^{-/-}$ mice were carried out as previously described (Cohen et al., 2014; Liu et al., 2003). All other animals were lean male mice (5 – 8 weeks of age) obtained from either The Jackson Laboratory (C57BL/6) or Taconic Biosciences (129SVE), unless otherwise noted. For mitochondrial purification, five to seven week old male (C57BL/6 or 129SVE) mice (15 - 20 mice total per experiment) were cold-exposed for one week, and used to obtain beige and brown fat mitochondria. Animal experiments were performed according to procedures approved by the Institutional Animal Care and Use Committee (IACUC) of the Beth Israel Deaconess Medical Center.

Breeding Schemes For Adipo-PRDM16 KO and *Ucp1*$^{-/-}$ Mice

Prdm16$^{lox/lox}$ and Adipo-PRDM16 KO mice were generated by breeding Adipoq-Cre transgenic mice (Eguchi et al., 2011) to *Prdm16*$^{lox/lox}$ mice in order to obtain *Prdm16*$^{lox/lox}$ and *Prdm16*$^{lox/lox}$;Cre genotypes, respectively as previously described (Cohen et al., 2014). *Ucp1*$^{-/-}$ mice and littermate *Ucp1*$^{+/+}$ controls were

generated by breeding male and female *Ucp1*$^{-/+}$ (B6.129-Ucp1tm1Kz/J) mice as described previously (Liu et al., 2003).

Crude Mitochondrial Isolation

The entire procedure of mitochondrial isolation was conducted at 4°C. Tissues were dissected and washed in ice-cold SHE buffer (250 mM sucrose, 10 mM HEPES, 0.1 mM EGTA, pH 7.2) to remove traces of blood and connective tissue. SHE buffer was supplemented with 2% essentially fatty acid free BSA during the isolation of brown fat and beige fat mitochondria. Tissues were minced on ice and homogenized in SHE buffer (5 ml g^{-1}) with a motorized Potter-Elvehjem teflon pestle. Homogenates were centrifuged at 8,500 g for 10 min. Supernatant was decanted rapidly to remove lipids. Pellet, containing cell debris, nuclei and mitochondria was resuspended and centrifuged at 700 g for 10 min to pellet nuclei and cell debris. The supernatant was transferred to a clean tube and centrifuged at 8,500 g for 10 min to pellet crude mitochondria. The mitochondrial pellet was washed with SHE buffer in a small volume to yield a concentration of roughly 25-50 mg ml^{-1} mitochondrial protein. Mitochondria were stored on ice and aliquots were removed as required during functional analyses.

Protease Protection Assay

Sucrose-purified mitochondria, isolated from cold-exposed (7 days) 129SVE mice, were incubated with varying amounts of trypsin (see figure legends for

details) for 30 minutes at room temperature. Mitochondria were treated rapidly with 1% SDS and boiled to denature proteins and subsequently used for Western blot analysis.

Mitochondrial Respiration

Mitochondrial respiration was determined using an XF24 Extracellular Flux Analyzer (Seahorse Bioscience) using 15 μg mitochondrial protein in a buffer containing 50mM KCl, 4mM KH2PO4, 5mM HEPES, and 1mM EGTA, 4% BSA, 10mM Pyruvate, 5mM Malate, 1mM GDP. Mitochondria were plated and centrifuged 2,000 g for 20 minutes to promote adherence to the XF24 V7 cell culture microplate. Uncoupled and maximal OCR was determined using Oligomycin (14 μM) and FCCP (10 μM). Rotenone and Antimycin A (4 μM each) were used to inhibit Complex 1- and Complex 3-dependent respiration. Creatine was added to a final concentration of 0.01 mM for most experiments, unless noted otherwise in the figure legend. "State 3" delineates the time (based on ADP titrations in Figure S2A) where the initial ADP-stimulated rate is similar to the rate achieved with 1 mM ADP. "ADP-limiting" delineates the time where the rate transitions to State 4.

Calculation of Creatine:ADP Stoichiometry

Creatine was added to mitochondria at a concentration of 0.01 mM in a total volume of 0.555ml in the XF well. Thus, the total pmoles of creatine in the entire

well was 5,550 pmoles. The XF microchamber volume during measurement of the oxygen consumption rate is 2 – 7µl. Based on a conservative estimate of a 7µl microchamber volume, this is equivalent to a total of 70 pmoles creatine in the microchamber. The total pmoles of oxygen consumed was measured over a 3 minute period, based on the oxygen consumption rate (measured as pmoles/min). The quantity of ADP molecules phosphorylated to ATP was calculated based on the mitochondrial P/O ratio (Watt et al., 2010).

Differential Scanning Calorimetry

Creatine-dependent heat production was measured using a MicroCal VP-DSC System (GE Healthcare), under the same buffer conditions as those used for mitochondrial respiration experiments, except for the ADP concentration, which was at 1 mM. The reason for increasing the ADP concentration was because of the increased time between additions of all components to the moment of measurement. The difference in thermogenesis was based on the maximal detected rightward shift in differential power between incubation with or without creatine.

Primary Inguinal Adipocyte Differentiation

Primary inguinal preadipocytes were counted and plated in the evening at 20,000 cells per well of a seahorse plate. The following morning inguinal preadipocytes were induced to differentiate with 1µM rosiglitazone, 0.5mM

isobutylmethylxanthine, 1μM dexamethasone, and 5 μg ml^{-1} insulin. Cells were re-fed every 48 hours with 1μM rosiglitazone and 5μg ml^{-1} insulin. Cells were fully differentiated by day 5 post-induction.

Primary Brown Adipocyte Differentiation

Primary brown preadipocytes were counted and plated in the evening at 15,000 cells per well of a seahorse plate. The following morning brown preadipocytes were induced to differentiate with 1μM rosiglitazone, 0.5mM IBMX, 5μM dexamethasone, 0.114μg ml^{-1} insulin, 1nM T3, and 125μM Indomethacin. Cells were re-fed every 48 hours with 1μM rosiglitazone and 0.5μg ml^{-1} insulin. Cells were fully differentiated by day 5 post-induction

Tissue Respiration

Tissue respiration was performed using a Clark-type oxygen electrode (Strathkelvin Instruments). Freshly isolated tissues were rapidly weighed and minced until homogenous. Tissue homogenates were placed in tissue respiration buffer (10 mM Na_2HPO_4, 2 mM KH_2PO_4, 2.7 mM KCl, 137 mM NaCl, 2 % essentially fatty acid free BSA, and supplemented with 1 mM sodium pyruvate, pH 7.4). OCR was measured at 37°C and normalized to tissue weight.

Whole Body Energy Expenditure

Animals were housed individually in metabolic chambers maintained at 23°C under a 12 hr light/dark cycle with free access to food and water. Whole body metabolic rate was measured using the Oxymax open-circuit indirect calorimeter, Comprehensive Lab Animal Monitoring System (CLAMS, Columbus Instruments). Movement was measured as the mean beam breaks per 35 minutes for 6 hours before CL 216,243 (Pre CL) and 6 hours after CL (Post CL) injection. Treatments are also outlined in the Figure Legends.

Mass Spectrometry: **Protein Extraction and Proteolytic Digestion**

Mitochondria enriched fractions were lysed with a dounce homogenizer with SDS lysis buffer [2% SDS w/v, 250 mM NaCl, EDTA free protease inhibitor cocktail (Promega, Madison, WI) and 50 mM HEPES, pH 8.5 at a 1:1 ratio. Fractions were reduced with 5 mM DTT for 30 minutes at 57°C, cooled for 15 min at RT and cysteine residues were alkylated with 14 mM iodoacetamide in the dark. Protein content was extracted by methanol-chloroform precipitation followed by two subsequent cold acetone washes. Protein pellets were air-dried and dissolved with 500 µl 8 M Urea containing 50 mM HEPES, pH 8.5. Protein concentrations were measured by BCA assay (Thermo Scientific, Rockford, IL) prior to protease digestion. Mitochondrial proteins were diluted to 4 M urea and digested with LysC (Wako, Japan) in a 1/200 enzyme/protein ratio overnight. Mitochondrial proteins were diluted further with 25 mM HEPES, pH 8.5 to a 1 M urea concentration and trypsin (Promega, Madison, WI) was added to a final

1/250 enzyme/protein ratio for 6 hr at 37°C. Digests were acidified with 250 µl of 20% formic acid (FA) to a pH ~ 2 and concentrated using C_{18} SPE on Sep-Pak cartridges (50 mg) (Sep-Pak, Waters, Milford, MA).

Tandem Mass Tagging and Labeling

Isobaric labeling of the enriched peptides was performed using 8-plex tandem mass tag (TMT) reagents (Thermo Fisher Scientific, Rockford, IL). TMT reagents (1 mg) were dissolved in 50 µl dry acetonitrile (ACN) and 10 µl was added to 100 µg of peptides dissolved in 100 µl of 200 mM HEPES, pH 8.5. After 1 hr at RT, the reaction was quenched by adding 4 µl of 5% hydroxylamine. TMT-labeled peptides were combined, acidified with 20 µl of FA and diluted to a final ~5% ACN concentration prior to C_{18} SPE on Sep-Pak cartridge (50 mg).

Basic pH Reversed-Phase HPLC (bpHrp)

TMT labeled mitochondrial peptides were subjected to orthogonal bpHrp fractionation. Labeled peptides were solubilized in 500 µl of buffer A (5% ACN 10 mM ammonium bicarbonate, pH 8.0) and separated by an Agilent 300 Extend C18 column (5 µm particles, 4.6 mm ID and 220 mm in length). Using an Agilent 1100 binary pump equipped with a degasser and a photodiode array (PDA) detector (Thermo Scientific, San Jose, CA), a 45 min linear gradient from 18% to 45% acetonitrile in 10 mM ammonium bicarbonate pH 8.0 (flow rate of 0.8 ml min^{-1}) separated the peptide mixtures into a total of 96 fractions. 96 fractions

were consolidated into 24 samples in a checkerboard manner, acidified with 10 µl of 20% FA prior to vacuum drying. Each sample was re-dissolved in 5% FA, desalted via StageTip desalting (3M Empore, South Eagan, MN), dried via vacuum centrifugation, and reconstituted in 5% FA/ 5% ACN prior to LC-MS/MS analysis.

Liquid Chromatography Separation and Tandem Mass Spectrometry (LC-MS/MS)

All LC-MS/MS experiments were performed on a LTQ Orbitrap-Velos Elite (Thermo Scientific) equipped Agilent 1200 binary HPLC pump (Agilent Technologies, Santa Clara, CA) and with a Famos autosampler (LC Packings, Sunnyvale, CA). Peptides were separated onto a 100 µm ID microcapillary column packed first with ~1 cm of Magic C4 resin (5 µm, 100 Å, Michrom Bioresources, Auburn, CA) followed by ~25 cm of Maccel C18AQ resin (3 µm , 200 Å, Nest Group, Southborough, MA). Separation was achieved through applying a gradient from 12 to 40% ACN in 0.5% FA over 170 min at ~250 nl min^{-1} flowrate. Electrospray ionization was enabled through applying a voltage of 1.8 kV using an inert gold electrode via a PEEK junction at the end of the microcapillary column.

The LTQ Orbitrap-Velos Elite was operated in data-dependent mode for the MS^3 method. For the MS^2 method, the survey scan was performed in the Orbitrap in the range of 400-1400 m/z at a resolution of $6x10^4$, followed by the

selection of the ten most intense ions (TOP 10) for HCD-MS^2 fragmentation using a precursor isolation width window of 2 m/z. The AGC settings were 3 x 10^6 and 2.5 x 10^5 ions for survey and MS^2 scans, respectively. Ions were selected for MS^2 when their intensity reached a threshold of 500 counts and an isotopic envelope was assigned. Maximum ion accumulation times were set to 1000 ms for survey MS scans and to 200 ms for MS^2 scans. The normalized collision energy for HCD-MS^2 experiments was set to 45% at a 30 ms activation time. Singly charged ion species and ions for which a charge state could not be determined were not subjected to a MS^2 scan. Ions within a 10 ppm m/z window around ions selected for MS^2 were excluded from further fragmentation for 90 s. The survey MS scan settings were identical for the MS^3 method, where the ten most intense ions were first isolated for ion trap CID- MS^2 at a precursor ion isolation width of 2 m/z, using an AGC setting of 2 x 10^3, a maximum ion accumulation time of 150 ms, and wide band activation. Directly following each MS^2 experiment, the most intense fragment ion in an m/z range between 110-160% of the precursor m/z was selected for HCD-MS^3. The fragment ion isolation width was set to 4 m/z, the MS^3 AGC was 20 x 10^4 and the maximum ion time 250 ms. Normalized collision energy was set to 35% and 55% at an activation time of 20 ms and 50 ms for MS/MS and MS^3 scans, respectively. Precursor ion selection settings were as in the MS^2 method.

Mass Spectrometry Data Processing and Spectra Assignment

A compilation of in-house software was used to convert mass spectrometric data (Raw file) to a mzXML format, as well as to correct monoisotopic m/z measurements and erroneous peptide charge state assignments. Assignment of MS/MS spectra was performed using the Sequest algorithm by searching the data against a protein sequence database including all entries in the Mouse Uniprot database (download date June, 2014) containing known contaminants such as human keratins and its reverse decoy components (Elias and Gygi, 2007). Sequest searches were performed using a 10 ppm precursor ion tolerance and requiring each peptide's N-/C- termini to have trypsin protease specificity, while allowing up to three missed cleavages. TMT tags on peptide N termini/lysine residues (+229.162932 Da) and carbamidomethylation of cysteine residues (+57.02146 Da) were set as static modifications while methionine oxidation (+15.99492 Da) was set as variable modification. A MS^2 spectra assignment false discovery rate (FDR) of less than 1% was achieved by applying the target-decoy database search strategy (Elias and Gygi, 2007). Filtering was performed using an in-house linear discrimination analysis algorithm to create one combined filter parameter from the following peptide ion and MS^2 spectra metrics: Sequest parameters XCorr and ΔCn, peptide ion mass accuracy and charge state, peptide length and missed-cleavages. Linear discrimination scores were used to assign probabilities to each MS^2 spectrum for being assigned correctly and these probabilities were further used to filter the dataset to a 1% protein-level FDR (Huttlin et al., 2010).

Determination of TMT Reporter Ion Intensities and Quantitative Data Analysis

For quantification, a 0.003 m/z window centered on the theoretical m/z value each of the eight reporter ions and the most intense signal intensity from the theoretical m/z value was recorded. Reporter ion intensities were further de-normalized based on their ion accumulation time for each MS^3 spectrum and adjusted based on the overlap of isotopic envelopes of all reporter ions as per manufacturer specifications. Total signal to noise values for all peptides were summed for each TMT channel, and all values were adjusted to account for variance in sample handling. For each peptide, a total minimum signal to noise value of 200 was required (McAlister et al., 2012; Ting et al., 2011).

Mass Spectrometry Data Analysis

The quantified proteins from the pure brown fat and beige fat mitochondrial preparations were clustered according to their relative expression via k-means. From the four primary clusters, one cluster of proteins exhibited elevated abundances in the beige adipose mitochondria and was selected for additional analysis. T-tests with Welch's correction for unequal variances was performed between beige fat and brown fat mitochondria. Multiple test correction was performed by adjusting the calculated p-values according to Benjamini-Hochberg (Benjamini and Hochberg, 1995).

Quantified proteins from the comparison of crude and pure extracts of beige and brown fat mitochondria were assessed for enrichment. Proteins exhibiting a mean relative fold change > 1 in the pure preparations were considered as mitochondrial-enriched. The mitochondrial-enriched subset of proteins was used as an additional filter for the comparison between brown and beige adipose mitochondria. Specifically. proteins exhibiting significant expression (adjusted p-value < 0.05) in the beige fat mitochondria were further filtered against the subset of proteins found to be enriched (ratio greater than 1) in the pure/crude mitochondrial enrichment experiment. The resulting subset of proteins was submitted for KEGG pathway enrichment (Huang da et al., 2009). All data analysis was performed using R (R Core Team, Vienna, Austria, http://www.R-project.org).

Gene Expression Analysis (qRT-PCR)

Total RNA was extracted from frozen tissue using TRIzol (Invitrogen), purified with RNeasy Mini spin columns (QIAGEN) and reverse transcribed using a High-Capacity cDNA Reverse Transcription kit (Applied Biosystems). The resultant cDNA was analyzed by qRT–PCR. Briefly, 20 ng cDNA and 150 nmol of each primer were mixed with SYBR GreenER^{TM} qPCR SuperMix (Applied Biosystems). Reactions were performed in a 384-well format using an ABI PRISM 7900HT real time PCR system (Applied Biosystems). Relative mRNA levels were calculated using the comparative CT method and normalized to *Ppib*

(for mouse) or *Tbp* (for human) mRNA. A complete list of primers and sequences can be found below.

Western Blotting

Samples were prepared in Adipocyte Lysis Buffer (50 mM Tris, pH 7.4, 500 mM NaCl, 1% NP40, 20% glycerol, 5 mM EDTA and 1 mM phenylmethylsulphonyl fluoride (PMSF), supplemented with a cocktail of Roche protease inhibitors). The homogenates were centrifuged at 16,000 g x 10 minutes at 4°C, and the supernatants were used for subsequent analyses. Protein concentration was determined using the bicinchoninic acid assay (Pierce). Quantity of protein lysate to use for each antibody was determined empirically. Protein lysates were denatured in Laemmli buffer (60 mM Tris, pH 6.8, 2% SDS, 10% glycerol, 0.05 % bromophenol blue, 0.7 M β-mercaptoethanol), resolved by 4-12% NuPAGE Bis-Tris SDS–PAGE (Invitrogen) and transferred to a polyvinylidene difluoride (PVDF) membrane. Primary antibodies were diluted in TBS containing 0.05% Tween (TBS-T), 5% BSA and 0.02% NaN_3. Membranes were incubated overnight with primary antibodies at 4°C. For secondary antibody incubation, anti-rabbit or anti-mouse HRP (Promega) was diluted in TBS-T containing 5% milk. Results were visualized with enhanced chemiluminescence (ECL) western blotting substrates (Pierce).

Antibodies

The following commercially available antibodies were used for Western blotting. TOM20 (Santa Cruz; sc-11415), Total OXPHOS (Abcam; ab110413), GATM (Abcam; ab119269), GAMT (Abcam, ab126736), CKMT2 (Abcam; ab55963), UCP1 (Abcam; ab10983), ACO2 (Abcam; ab110321), VDAC (Abcam; ab34726), VCL (Cell Signaling; 13901), PHOSPHO1 (Abcam; ab130991), PHOSPHO2 (Abcam; ab156078), GAPDH (Abcam; ab8245), CLNX (Abcam; ab22595), KDEL (Abcam; ab12223), PGAM5 (Abcam; ab126534), HMGCS2 (Abcam; ab137043), COX5B (Abcam; ab110263),

Mouse qRT-PCR Primer Sequences

Ppib Fwd: 5'-GGA GAT GGC ACA GGA GGA A-3', Rev: 5'-GCC CGT AGT GCT TCA GCT T-3'; ***Fabp4*** Fwd: 5'-AAG GTG AAG AGC ATC ATA ACC CT-3', Rev: 5'-TCA CGC CTT TCA TAA CAC ATT CC-3'; ***Pparg2*** Fwd: 5'-TGC CTA TGA GCA CTT CAC AAG AAA T-3', Rev 5'-CGA AGT TGG TGG GCC AGA A-3'; ***Ucp1*** Fwd: 5'-ACT GCC ACA CCT CCA GTC ATT-3', Rev: 5'-CTT TGC CTC ACT CAG GAT TGG-3'; ***Dio2*** Fwd: 5'-CAG TGT GGT GCA CGT CTC CAA TC-3', Rev 5'-TGA ACC AAA GTT GAC CAC CAG-3'; ***Slc6a8*** Fwd: 5'-TGC ATA TCT CCA AGG TGG CAG-3', Rev: 5'-CTA CAA ACT GGC TGT CCA GA-3'; ***Gatm*** Fwd: 5'-GAC CTG GTC TTG TGC TCT CC-3', Rev: 5'- GGG ATG ACT GGT GTT GGA GG-3'; ***Gamt*** Fwd: 5'- GCA GCC ACA TAA GGT TGT TCC-3', Rev 5'- CTC TTC AGA CAG CGG GTA CG-3'; ***Ckmt1*** Fwd: 5'- TGA GGA GAC CTA TGA GGT ATT TGC-3', Rev: 5'- TCA TCA AAG TAG CCA GAA CGG A-3';

Ckmt2 Fwd: 5'-GCA TGG TGG CTG GTG ATG AG-3', Rev 5'- AAA CTG CCC GTG AGT AAT CTT G-3'; ***Phospho1*** Fwd: 5'- AAG CAC ATC ATC CAC AGT CCC TC-3', Rev: 5'- TTG GTC TCC AGC TGT CAT CCA G-3'; ***Phospho2*** Fwd: 5'- AGG TGA AGG ACA GCC CTT TG-3', Rev: 5'- ATG CAG CAA AGG AAC AAA GAC-3'; ***Fhit*** Fwd: 5'-GCT TTG AAG CCC AGC AAA GAA-3', Rev 5'- TCA CAG TAA AAG CTC CTT GGG G-3'; ***Pgam5*** Fwd: 5'- AAG ATG GAG CCC GGA TTG AAG-3', Rev: 5'- TTC TGG GGG AAA CTG CAA CG-3'; ***Lpin1*** Fwd: 5'- TCG TGG TCA AGG TTG GCA AT-3', Rev 5'- ATT CCA CAG TGG CCT TTG GC-3'; ***Ak3*** Fwd: 5'- CAG AAC ATG CTG CAG GGC AC-3', Rev: 5'- GGA AAT CCA TCC AAC AGC CAG CTA-3'; ***Ptpn1*** Fwd: 5'- ACT GGG CGG CTA TTT ACC AG-3', Rev: 5'-CTG TGG TCA AAA GGG CTG AC-3'; ***Acp6*** Fwd: 5'- CAC CAG TCT ACA ACC CCC AAG-3', Rev 5'- GGA TGA CGG CAG ACC CTT TC-3'; ***Pdp1*** Fwd: 5'-AGG AGA ATG TGT GTG TGT CCC-3', Rev: 5'- AGA GAA CAG TGG CAG ACT GG-3'; ***Pptc7*** Fwd: 5'-GAC GAC GCG TGT TTC GTG-3', Rev 5'-ACT AAC CGC TCG CAT GTT CG-3'; ***Nudt9*** Fwd: 5'- ATA ACC AGG TGG AAA AGG GAC G-3', Rev: 5'- ACT GAT CTT CTC TCC GGG GT-3'; ***Pdpr*** Fwd: 5'-ACC TGG AAA TAC ACA GCC CT-3', Rev 5'-CCC ATT TGC ATA GCC CAC AC-3';

Human qRT-PCR Primer Sequences

Tbp Fwd: 5'- CAC GAA CCA CGG CAC TGA TT -3', Rev: 5'- TTT TCT TGC TGC CAG TCT GGA C -3'; ***Ckmt1*** Fwd: 5'- TGA GGA GAC CTA TGA GGT ATT

TGC -3', Rev: 5'- CTC ATC AAA GTA GCC AGA ACG G -3'; ***Ckmt2*** Fwd: 5'- AGG AGT CCT ATG AGG TGT TTG C -3', Rev: 5'- CGT AAT GCT CGT CGA ACT GC -3'; ***Phospho1*** Fwd: 5'- ATA CCT CAG CTA GCC CCC TT -3', Rev: 5'- TTG TCG GTG CAT TAC CGT GA -3'; ***Ucp1*** Fwd: 5'- GTG TGC CCA ACT GTG CAA TG -3', Rev: 5'- CCA GGA TCC AAG TCG CAA GA -3'; ***Pgc-1α*** Fwd: 5'- CTG TGT CAC CAC CCA AAT CCT TAT -3', Rev: 5'- TGT GTC GAG AAA AGG ACC TTG A -3'; ***Pparg*** Fwd: 5'- AGC CTC ATG AAG AGC CTT CCA -3', Rev: 5'- TCC GGA AGA AAC CCT TGC A -3'; ***Dio2*** Fwd: 5'- TCC AGT GTG GTG CAT GTC TC -3', Rev: 5'- CTG GCT CGT GAA AGG AGG TC -3'

Adipocyte Culture

Primary inguinal and brown stromal vascular fraction preparation, culture, and differentiation can be found in Extended Experimental Procedures. Human brown adipocytes were prepared, cultured and differentiated (with 1μM rosiglitazone) as described (Shinoda et al., 2015).

Creatine Kinase Activity

Creatine kinase activity from sucrose-gradient isolated mitochondria (0.25μg total protein) and serum samples (1 μl) was examined using the Creatine Kinase Activity Assay Kit (Sigma) according to the manufacturer's instructions.

Creatine and Phosphocreatine (PCr) Measurements

Creatine content was measured fluorometrically using a Creatine Assay Kit (Sigma), according to the manufacturer's instructions. PCr was determined using a Mouse Creatine Phosphate ELISA (Biotrend Gmbh), according to the manufacturer's instructions.

Body Temperature

A mouse rectal probe (World Precision Instruments) was used to examine body temperature. Body temperature was measured within 1 – 2 hours following β-GPA (0.4 g kg^{-1}) injection at zeitgeber time (ZT) 8 to 10.

Primary Inguinal Stromal Vascular Fraction Preparation

Inguinal stromal vascular fraction (SVF) was obtained from 4-6 week old mice. Inguinal adipose was dissected, washed in PBS, minced, and digested for 45 minutes at 37 °C in PBS containing 10 mg ml^{-1} collagenase D (Roche), 3 U ml^{-1} dispase II (Roche), and 10 mM $CaCl_2$. Tissue suspension was filtered through a 100 µm cell strainer and centrifuged at 600 g for 5 min to pellet the SVF. The cell pellet was resuspended in adipocyte culture medium (DMEM/F12 with GlutaMAX (1:1, Invitrogen), 10 % FBS and 0.1 % PenStrep), filtered through a 40 µm cell strainer, centrifuged at 600 g for 5 min, resuspended and plated in adipocyte culture medium.

Primary Brown Stromal Vascular Fraction Preparation

Interscapular brown adipose SVF was obtained from 2-6 day old pups. Interscapular brown adipose was dissected, washed in PBS, minced, and digested for 45 minutes at 37 °C in PBS containing 1.5 mg ml^{-1} collagenase B (Roche), 123 mM NaCl, 5 mM KCl, 1.3 mM $CaCl_2$, 5 mM glucose, 100 mM HEPES, and 4 % essentially fatty acid-free BSA. Tissue suspension was filtered through a 100 µm cell strainer and centrifuged at 600 g for 5 min to pellet the SVF. The cell pellet was resuspended in adipocyte culture medium (DMEM/F12 with GlutaMAX (1:1, Invitrogen), 10 % FBS and 0.1 % PenStrep), filtered through a 40 µm cell strainer, centrifuged at 600 g for 5 min, resuspended and plated in adipocyte culture medium.

Adenoviral shRNA Cloning, Construction, and Use

Complementary DNA oligos for shRNA generation were annealed and cloned into the pENTR™/U6 entry vector according to the manufacturer's instructions (Invitrogen; K4944). Sequences for shRNA targeting were as follows: ***Phospho1-#1*** sense: CAC CGG CTC CTG CTT CGA GGT TAT TCG AAA ATA ACC TCG AAG CAG GAG CC; antisense: AAA AGG CTC CTG CTT CGA GGT TAT TTT CGA ATA ACC TCG AAG CAG GAG CC; ***Phospho1-#2*** sense: CAC CGT ACG TGG GTG ATG GTG CAA ATC GAA ATT TGC ACC ATC ACC CAC GTA; antisense: AAA ATA CGT GGG TGA TGG TGC AAA TTT CGA TTT GCA CCA TCA CCC ACG TAC; ***LacZ*** sense: CAC CGC TAC ACA AAT CAG CGA TTT CGA AAA ATC GCT GAT TTG TGT AG, antisense: AAA ACT ACA CAA

ATC AGC GAT TTT TCG AAA TCG CTG ATT TGT GTA GC. Cloned shRNA's were shuttled into the pAD/BLOCK-iT™-DEST Gateway® vector and transfected into 293A cells. Crude adenovirus was generated according to the manufacturer's instructions (Invitrogen; K4941). Crude adenovirus was amplified by infecting 293A cells, and purified using the Fast Trap Adenovirus Purification and Concentration Kit (EMD Millipore), according to the manufacturer's instructions. Primary adipocytes were transduced with purified adenovirus ($5x10^6$ pfu) in the evening of day 1 and then again in the evening at day 3 of differentiation, with medium replacement the following morning each time.

RNAi-mediated Human Gene Knockdown

Individual siRNA pools (SMARTpool) for *Ckmt1* (no. 049314) and non-targeting siRNA control (no. 001810) were obtained from GE Dharmacon. Clonal human brown afipocyte (Shinoda et al., 2015), line #1 was used for RNAi-mediated knockdown. siRNA was reverse transfected with Lipofectamine RNAiMAX (following the manufacturere's protocol) at day 0 of differentiation and then forward transfected once every five days. Cells were harvested at day 21 post-differentiation.

Electromyography (EMG)

Mice were placed in a restrainer to limit free movement. Needle electrodes were placed subcutaneously, close to the back muscles near the neck, to measure

muscle activity. EMG data were collected from the implanted electrodes at a sampling rate of 2 kHz using LabChart 8 Pro Software (ADInstruments, Colorado Springs, CO). The raw signal was converted to root mean square (RMS) activity. RMS activity was analyzed for shivering bursts in 10s windows. A burst was defined when RMS activity exceeded a threshold (set at 25 μV above the baseline level) for at least 200 ms. The baseline was defined as the mean EMG signal within the entire measurement window. Shivering was inhibited with a single intraperitoneal injection of D-tubocurarine (0.3 mg kg^{-1} for females). This dose of D-tubocurarine was not toxic, as mice fully recovered 2 hours post-injection.

PHOSPHO1 Purification

A plasmid (pBAD-TOPO-TA) containing the cDNA corresponding to Met^{19} – Cys^{267} of human PHOSPHO1 (hPHOSPHO1) was a kind gift from Dr. Colin Farquharson. A culture of *E. coli* cells (1 Liter) containing hPHOSPHO1 cDNA was grown to an OD_{600} of 0.8 and recombinant protein expression was induced by treatment with 0.1% (w/v) L-arabinose for four hours at 37°C. Bacteria were harvested by centrifugation at 6,500 g x 15 minutes and pellets were frozen at -80°C. On the day of purification, bacteria were thawed on ice and resuspended in Buffer P1 (50 mM $NaPO_4$ [pH 8.0], 300 mM NaCl, 10 mM Imidazole, supplemented with a protease inhibitor cocktail (P.I.C.) consisting of 1 mg/ml leupeptin, 2 mg/ml antipain, 10 mg/ml benzamidine, 5 TIU/ml aprotinin, 1 mg/ml

chymostatin, 1 mg/ml pepstatin, and 1 mM AEBSF). Cells were lysed at 4°C by sonication (30 sec on / 30 sec off, 60% power, for a total of 5 minutes) using a Misonix S4000. Lysates were clarified by centrifugation at 7,000 g x 30 minutes and filtration (0.2 µm membrane). A column volume (1 ml) of Ni Sepharose beads was equilibrated in Buffer P1 and incubated with clarified lysate for 1.5 hours at 4°C, rolling end over end. The bead/lysate mixtures was added to a gravity column and the lysate was collected as the flow-through fraction. Next, the column was washed with ten bed volumes of Buffer P2 (50 mM Tris [pH8.0], 150 mM NaCl, 20 mM Imidazole, supplemented with P.I.C.). hPHOSPHO1 was eluted with three bed volumes of Buffer P3 (50 mM Tris [pH8.0], 150 mM NaCl, 250 mM Imidazole, supplemented with P.I.C.). Protein was dialyzed two times in Buffer P4 (50 mM Tris [pH7.2], 150 mM NaCl, 50 % Glycerol) overnight using 2 liters total (2L, 4°C, 16 hours). Protein was collected from dialysis tubing and maintained on ice to examine activity. Remaining hPHOSPHO1 was flash frozen in liquid nitrogen and stored at -80°C.

Purine Nucleoside Phosphorylase (PNPase)-Coupled Phosphatase Assay

A spectrophotometric method was used to monitor the continuous release of inorganic phosphate, using the EnzChek® Phosphate Assay Kit (Molecular Probes). Reactions were measured in quadruplicate using 5 µg PHOSPHO1 protein in 96-well plates at 37°C containing Phospho1 buffer (20 mM Mes, 0.01% de-fatted BSA, 0.013% (v/v) Tween-20), 0.2 units PNPase, 200 µM MESG (2-

amino-6-mercapto-7-methylpurine ribonucleoside), and supplemented with various divalent metals to 2 mM. Absorbance was measured continuously at 355 nm using a FLUOstar Omega plate reader.

Statistical Analysis

Results are presented as mean ±SEM. Unpaired two-tailed Student's t test and two-way ANOVA were used to determine statistical differences. Significance was considered as $p < 0.05$.

Supplementary Table S3, Related to Figure 1.
Beige Fat Enriched Proteins, Kegg Pathway: Arginine/Creatine and Proline Metabolism

Protein Name	Gene Symbol	Beige C57BL/6	Brown C57BL/6	Beige 129SVE	Brown 129SVE	C57BL/6 (Beige/ Brown)	129SVE (Beige/ Brown)
Creatine kinase U-type, mitochondrial	*Ckmt1*	31.14	6.70	31.46	9.34	4.65	3.37
Pyrroline-5-carboxylate reductase 2	*Pycr2*	1676.50	595.22	1226.25	655.61	2.82	1.87
Glutamine synthetase	*Glul*	3480.80	1515.54	2934.60	1862.91	2.30	1.58
Proline dehydrogenase 1, mitochondrial	*Prodh*	4607.86	2819.75	5377.88	3039.24	1.63	1.77
Creatine kinase B-type	*Ckb*	274.72	143.41	215.89	154.94	1.92	1.39
Glutamate dehydrogenase 1, mitochondrial	*Glud1*	12440.20	8517.18	13229.25	8681.35	1.46	1.52
Isoform IIa of Prolyl 4-hydroxylase subunit alpha-2	*P4ha2*	62.68	15.48	83.27	22.46	4.05	3.71
Isoform 2 of Alpha-aminoadipic semialdehyde dehydrogenase	*Aldh7a1*	2201.82	205.93	1721.55	337.77	10.69	5.10
Glycine amidinotransferase, mitochondrial	*Gatm*	543.60	83.01	864.44	125.17	6.55	6.91
Ornithine aminotransferase, mitochondrial	*Oat*	2078.15	560.42	1789.00	802.56	3.71	2.23
Isoform Short of Delta-1-pyrroline-5-carboxylate synthase	*Aldh18a1*	1055.35	164.33	1059.22	225.87	6.42	4.69
Pyrroline-5-carboxylate reductase 1, mitochondrial	*Pycr1*	338.32	45.20	329.13	65.22	7.49	5.05
Aldehyde dehydrogenase, mitochondrial	*Aldh2*	17081.40	8194.47	14156.55	8361.85	2.08	1.69
Creatine kinase S-type, mitochondrial	*Ckmt2*	361.64	289.49	651.50	291.18	1.25	2.24

SUPPLEMENTAL TABLE LEGENDS

Table S3. Beige Fat Enriched Proteins, Kegg Pathway: Arginine/Creatine and Proline Metabolism

Average quantification of proteins from beige and brown fat mitochondria from C57BL/6 and 129SVE mice (from Table S1) involved in Arginine/Creatine and Proline metabolism (Kegg pathway).

SUPPLEMENTAL REFERENCES

Benjamini, Y., and Hochberg, Y. (1995). Controlling the false discovery rate: a practical and powerful approach to multiple testing. J Roy Statist Soc Ser B *57*, 289-300.

Cohen, P., Levy, J.D., Zhang, Y., Frontini, A., Kolodin, D.P., Svensson, K.J., Lo, J.C., Zeng, X., Ye, L., Khandekar, M.J.*, et al.* (2014). Ablation of PRDM16 and beige adipose causes metabolic dysfunction and a subcutaneous to visceral fat switch. Cell *156*, 304-316.

Eguchi, J., Wang, X., Yu, S., Kershaw, E.E., Chiu, P.C., Dushay, J., Estall, J.L., Klein, U., Maratos-Flier, E., and Rosen, E.D. (2011). Transcriptional control of adipose lipid handling by IRF4. Cell metabolism *13*, 249-259.

Elias, J.E., and Gygi, S.P. (2007). Target-decoy search strategy for increased confidence in large-scale protein identifications by mass spectrometry. Nature methods *4*, 207-214.

Huang da, W., Sherman, B.T., and Lempicki, R.A. (2009). Systematic and integrative analysis of large gene lists using DAVID bioinformatics resources. Nature protocols *4*, 44-57.

Huttlin, E.L., Jedrychowski, M.P., Elias, J.E., Goswami, T., Rad, R., Beausoleil, S.A., Villen, J., Haas, W., Sowa, M.E., and Gygi, S.P. (2010). A tissue-specific atlas of mouse protein phosphorylation and expression. Cell *143*, 1174-1189.

Liu, X., Rossmeisl, M., McClaine, J., Riachi, M., Harper, M.E., and Kozak, L.P. (2003). Paradoxical resistance to diet-induced obesity in UCP1-deficient mice. The Journal of clinical investigation *111*, 399-407.

McAlister, G.C., Huttlin, E.L., Haas, W., Ting, L., Jedrychowski, M.P., Rogers, J.C., Kuhn, K., Pike, I., Grothe, R.A., Blethrow, J.D.*, et al.* (2012). Increasing the multiplexing capacity of TMTs using reporter ion isotopologues with isobaric masses. Analytical chemistry *84*, 7469-7478.

Shinoda, K., Luijten, I.H., Hasegawa, Y., Hong, H., Sonne, S.B., Kim, M., Xue, R., Chondronikola, M., Cypess, A.M., Tseng, Y.H.*, et al.* (2015). Genetic and functional characterization of clonally derived adult human brown adipocytes. Nature medicine *21*, 389-394.

Ting, L., Rad, R., Gygi, S.P., and Haas, W. (2011). MS3 eliminates ratio distortion in isobaric multiplexed quantitative proteomics. Nature methods *8*, 937-940.

Watt, I.N., Montgomery, M.G., Runswick, M.J., Leslie, A.G., and Walker, J.E. (2010). Bioenergetic cost of making an adenosine triphosphate molecule in animal mitochondria. Proceedings of the National Academy of Sciences of the United States of America *107*, 16823-16827.